xFitter: An Open Source QCD Analysis Framework

A resource and reference document for the Snowmass study

(xFitter Collaboration)[*]

The xFitter Developers' Team:, H. Abdolmaleki [ID], S. Amoroso [ID], V. Bertone [ID], M. Botje [ID],
D. Britzger [ID], S. Camarda [ID], A. Cooper-Sarkar [ID], J. Fiaschi [ID], F. Giuli [ID], A. Glazov [ID],
C. Gwenlan [ID], F. Hautmann [ID], H. Jung [ID], A. Kusina [ID], A. Luszczak [ID], T. Mäkelä [ID],
I. Novikov [ID], F. Olness [ID], R. Sadykov [ID], P. Starovoitov [ID], M. Sutton [ID], and O. Zenaiev [ID]

(Dated: 15 March 2022)

We provide an overview of the xFitter open-source software package, review the general capabilities of the program, and highlight applications relevant to the Snowmass study. An updated version of the program (2.2.0) is available on CERN GitLab,[a] and this has been updated to a C++ codebase with enhanced and extended features. We also discuss some of the ongoing and future code developments that may be useful for precision studies. We survey recent analyses performed by the xFitter developers' team including: W and Z production, photon PDFs, Drell-Yan forward-backward asymmetry studies, resummation of small-x contributions, heavy quark production, constraints on the strange PDF, determination of the pion PDF, and determination of the pion Fragmentation Functions. Finally, we briefly summarize selected applications of xFitter in the literature. The xFitter program is a versatile, flexible, modular, and comprehensive tool that can provide impact studies for possible future facilities. We encourage the use of xFitter, and welcome new contributions from the community.

CONTENTS

I. INTRODUCTION TO xFitter

A. xFitter Overview

xFitter [1] (formerly **HERAfitter**) is an open-source software package that provides a framework for the determination of the **parton distribution functions** (PDFs) of the proton and related subjects.[1] xFitter version 2.0.1 is currently available, and version 2.2.0 will be released imminently and offers an expanded set of tools and options. It incorporates experimental data from a wide range of experiments including fixed-target, Tevatron, HERA, and LHC data sets. xFitter can analyze this data using predictions up to next-to-next-to-leading-order (NNLO) in perturbation theory with a variety of theoretical calculations including numerous methodological options for carrying out PDF fits and plotting tools which help visualize the results. While primarily based on the collinear factorization foundation, xFitter also provides facilities for fits of dipole models and **transverse-momentum dependent** (TMD) distributions. The package can be used to study the impact of new precise measurements from hadron colliders, and also assess the impact of future colliders. This paper provides a brief overview of xFitter with emphasis of the features relevant for the Snowmass2021 study.

The need for precision PDFs: The PDFs are the essential components that allow us to make theoretical predictions for experimental measurements of collider experiments with initial state protons and hadrons. Despite the recent progress of PDF analyses (including NLO and NNLO calculations), the uncertainty for many precision measurements at the LHC stems nowadays primarily from the PDFs [2–4]. Hence, our ability to fully characterize the Higgs boson and constrain Beyond-Standard-Model (BSM) physics signatures ultimately comes down to how accurately we determine the underlying PDFs; this is the focus of the xFitter project.

Open Source Code: The xFitter package is provided at `www.xFitter.org`, and a write-up of the program can be found in Ref. [1], and an overview of available tutorials in Ref. [5] including some presented at MCnet-CTEQ schools. The xFitter framework has already been used for more than 100+ analyses including many LHC studies. The code structure of the xFitter package is modular, and it allows for various theoretical and methodological options. Currently it contains interfaces to QCDNUM [6], APFEL [7, 8], LHAPDF [9], APPLGRID [10], APFELGRID [11], FastNLO [12], HATHOR [13], among other packages.

xFitter also has a large number of data sets available, including a variety of fixed target experiments, HERA,

Tevatron, and LHC. It is also possible to add new custom data sets such as LHeC [14] and EIC [15, 16]) pseudo-data.

B. xFitter Capabilities

PDF Fits & Analysis: First and foremost, xFitter provides a flexible open-source framework for performing PDF fits to data. The PDFs are the fundamental object that xFitter works with, and it has a variety of utilities to read, write, and manipulate the standardized PDF file format and associated uncertainties. For example, xFitter is able to read and write PDFs in the LHAPDF6 format [9].

xFitter-draw: xFitter can also automatically generate comparison plots of data vs. theory. There are a variety of options for the definition of the χ^2 function and the treatment of experimental uncertainties. Examples are presented in Ref. [1].

Nuclear PDFs: xFitter has also been extended to produce nuclear PDFs; this was used to produce the TUJU19 nPDF set of Ref. [17].

Pion PDFs: xFitter can also produce meson PDFs, and Ref. [18] illustrates this for the case of pion PDFs.

Pseudo-Data: An important application of xFitter is to understand how a particular data set or experiment will impact the PDFs. A typical study might be to use pseudo-data from a proposed experiment (e.g. LHeC or EIC) to constrain the relative uncertainty on the underlying PDFs. For example, Ref. [19] used LHeC pseudo-data to constrain the strange PDF with charged-current DIS charm production data. Additionally, forward-backward Drell-Yan asymmetry pseudo-data were prepared to simulate the end of Run-II LHC (i.e. $300\ fb^{-1}$), and also the HL-LHC; these pseudo-data have been used for PDF profiling in Refs. [3] and [20].

Profiling & Reweighting: xFitter is able to perform PDF profiling and reweighting studies. The reweighting method allows xFitter to update the probability distribution of a PDF uncertainty set (such as a set of NNPDF replicas) to reflect the influence of new data. For the PDF profiling, xFitter compares data and MC predictions based on the χ^2-minimization, and then constrains the individual PDF eigenvector sets taking into account the data uncertainties. For example, Ref. [2] used the Tevatron W-boson charge asymmetry and of the Z-boson production cross sections data to study the impact on the PDFs using Hessian profiling and Bayesian reweighting techniques.

In a separate study [3], the forward-backward asymmetry in neutral current Drell-Yan production provides powerful constraints on the valence quark PDFs, and this in turn can impact both SM [21, 22] and BSM [23, 24] physics.

---

[1] The xFitter program is available on the web at: www.xFitter.org

NNLO & QED PDFs: As many PDF analyses are now extended out to NNLO, the NLO QED effects can also become important. For example, including QED processes in the parton evolution will break the isospin symmetry as the up and down quarks have different couplings to the photon. xFitter is able to include NLO QED effects, and this is illustrated in Ref. [25] which computes the photon PDF as determined using a NNLO QCD and NLO QED analysis.

Transverse-momentum-dependent distributions: Transverse-momentum-dependent (TMD) parton distribution functions [26] encode nonperturbative information on hadron structure, extending to the transverse plane the one-dimensional picture given by collinear PDFs, and providing a 3D imaging of hadron structure. Similarly to collinear PDFs, TMDs can be parameterised and fitted to experimental data. Within the xFitter framework, the extraction of TMDs from fits to experimental data has been carried out in the cases of CCFM evolution [27–29] and Parton Branching evolution [30–32]. xFitter is able to write and manipulate TMDs in the TMDlib format [33, 34].

Small-x resummation: xFitter can also study the impact of the $\ln(1/x)$-resummation corrections to the DGLAP splitting functions and DIS coefficient functions. The resummation formalism for both the splitting functions and the coefficient functions is developed in [35]. The Leading-Log $\ln(1/x)$ (LLx) [36–39] and Next-to-Leading-Log $\ln(1/x)$ (NLLx) [35, 40–42] resummed calculations are implemented in the public code HELL [43, 44]. The phenomenological effects of the $\ln(1/x)$ resummation are investigated in Ref. [45]. In a related study [46], a more flexible PDF parameterisation is used with xFitter which provides a better description of the combined inclusive HERA I+II data, expecially at low x.

Pole & $\overline{MS}$ running masses: Another feature of xFitter is the ability to handle both pole masses and $\overline{MS}$ running masses. While the pole mass is more closely connected to what is measured in experiments, the $\overline{MS}$ mass has advantages on the theoretical side of improved perturbative convergence. xFitter was used to perform a high precision determination of the $\overline{MS}$ charm mass in this new framework [47].

Dipole models: We have several dipole models [48–50] implemented in xFitter which describe HERA inclusive and diffractive DIS cross sections very well and are a natural description of QCD reaction in the low x and low Q^2 region, fits to HERA data are shown in [51, 52]. The gluon distribution [52] determined from dipole model in xFitter can be applied to the description of selected LHC processes such as gamma-proton and nucleus-nucleus collisions [53, 54].

C. xFitter and Snowmass2021

We briefly discuss how xFitter might contribute to some of the future projects being studied in the Snowmass2021 planning process.

LHC & HL-LHC: The xFitter package has been used for more than 100 analyses including many LHC studies; a more complete list is available at `www.xFitter.org`. Applying this work to data taken at HL-LHC is a natural extension.

To highlight just one LHC example, the strange quark PDF has generated considerable attention in the recent literature. There is a comprehensive study [55] that examines the compatibility of both the ATLAS [56, 57] and CMS [58] data in a uniform framework using the xFitter program.

EIC & LHeC: The EIC [59] and LHeC [14] facilities will provide lepton–nucleon scattering in a collider configuration with a variety of beams.

In addition to exploring the proton PDFs, these colliders can also study nuclear PDFs with nuclear beams, and also meson (pion & kaon) structure via leading neutron production. xFitter is capable of studying both nuclear PDFs [17] and meson PDFs [18]. Additionally, xFitter can also compute the transverse momentum dependent (TMD) distributions [1].

DUNE: The Deep Underground Neutrino Experiment (DUNE) will use an intense neutrino beam generated at Fermilab to study open questions about neutrino oscillations. The massive DUNE detectors will also contribute to the study of proton decay and Grand Unified Theories, as well as observe neutrino signals from supernova core-collapse [60].

In particular, the NuSTEC white paper [61] outlines the status and challenges of neutrino-nucleus interactions, with special attention to DUNE. Improvements in PDF nuclear correction factors and the generation of nuclear PDFs fit, specifically to neutrino–nucleus interactions in the relevant energy range, can help minimize systematic errors for the +30% fraction of DUNE events coming from the DIS region. This would enhance analyses in both the near and far detectors. Thus, improvements by xFitter on both proton and nuclear PDFs [17] can contribute to the DUNE project.

UHE Cosmic Rays Recent advances in neutrino astronomy have enabled us to study ultra-high energy cosmic rays (UHECR) by studying atmospheric neutrinos. For example, IceCube [62, 63] has isolated more than 100 high-energy cosmic neutrinos, with energies between 100 TeV and 10 PeV.

Interpretation of these measurements would benefit from accurate PDFs in the low-x region. An example application is the evaluation of the prompt flux of atmospheric neutrinos originating from the semileptonic decays of heavy-flavored hadrons produced in the interactions of UHECR with nuclei in the atmosphere [64,

65]. The prompt atmospheric-neutrino flux represents a relevant background for searches of highly energetic cosmic neutrinos. Thus, increased precision of both PDFs and nuclear corrections in the very low-x region would improve theoretical predictions in this extreme kinematic region.

II. FUTURE DEVELOPMENTS WITH xFitter

The latest xFitter release, 2.2.0, represents a significant restructuring of the code. The new version provides significantly improved modularity for PDF parameterization, evolution, theory predictions and minimization. This additional flexibility simplifies further developments of the code.

The planned developments contain improvements of the existing functionality and expansion of the code capabilities. Both goals will be achieved in a modular manner, without increase of the requirements for the core package. An emphasis is given on usage of modern, industry-standard libraries.

There are several ideas on improvement of the execution time required for minimization. This is important in particular in view of large amount of data samples which will come from LHC, EIC, and other experiments. xFitter already contains an interface to the FK-tables ("apfelgrid") via interface to APFEL. These tables are based on APPLGRID predictions and combine evolution and convolution in one step. The interface to modern minimization packages, such as CERES [66], which is included in version 2.2.0, provides additional opportunity to employ automatic differentiation. Introduction of this capability is planned for the next release. Combined with improved minimization code, this should improve convergence time for specific problems by more that order of magnitude.

xFitter already contains highly efficient code for likelihood function calculation. It will be improved further, by more extensive use of BLAS and EIGEN libraries.

The state-of-the-art PDF fits include NNLO QCD plus NLO electroweak corrections. However, in many cases these corrections are provided as fixed k-factor tables. It is planned to include them using grid-based methods or with semi-analytic routines [67, 68].

xFitter plans further developments beyond conventional PDFs. In particular, the TMDs which have already been introduced through the parton branching method [31] will be developed by including branching scale-dependent resolution parameters [69] as a new functionality. Furthermore, TMDs will also be introduced independently of the parton branching method using the existing interface to the DYTURBO [70] package. It is also planned to introduce functionality for simultaneous PDF and fragmentation function fits.

The inclusion of theoretical uncertainties in PDFs is currently one of the main targets of state-of-the-art PDF global fits. xFitter plans to provide PDF sets incorporating theoretical uncertainties by applying the resummation-scale technique [71, 72].

NLO EW corrections are important at the precision level of the Drell-Yan measurements at the LHC and the Tevatron. Complete one-loop EW corrections for NC and CC Drell-Yan processes are realized in ReneSANCe Monte Carlo event generator that uses the SANC modules for differential cross-sections. The predictions obtained by ReneSANCe were thoroughly cross-checked with the results of MCSANC integrator. The complete one-loop EW corrections can be separated in the code into weak, QED FSR, QED ISR and interference (IFI) contributions. The dominant part of the higher-order EW corrections is QED FSR which can be modelled by PHOTOS program. The effects of QED FSR calculated by PHOTOS and ReneSANCe agree very well. The K-factors for the remaining parts of NLO EW can be computed with ReneSANCe for various differential cross sections, A_{FB} and charge asymmetries: $K^{\text{EW}} = \frac{d\sigma^{\text{NLO EW}}_{\text{LO QCD}}}{d\sigma^{\text{LO EW}}_{\text{LO QCD}}}$. In factorized approach this K-factors applies to NNLO QCD cross-sections: $d\sigma^{\text{NLO EW}}_{\text{NNLO QCD}} = d\sigma^{\text{LO EW}}_{\text{NNLO QCD}} \cdot K^{\text{EW}}$.

In the case of NC DY the separation of the FSR contribution is straightforward and appears at the level of Feynman diagrams. But the corresponding separation in the case of CC DY is not trivial and it is even not gauge invariant. For the sake of agreement with PHOTOS, a special prescription for this separation was introduced in SANC modules.

A formal separation of the pure weak (PW) and QED contributions δ^{PW} and δ^{QED} to the total $W^+ \rightarrow u + \bar{d}$ decay width $\Gamma^{PW+QED}_W = \Gamma^{LO}_W(\delta^{PW} + \delta^{QED})$ is depend on 't Hooft scale parameter μ_{PW} and $\delta^{QED} = \frac{\alpha}{pi}\left[Q^2_W(\frac{11}{6} - \frac{\pi^2}{3}) + (Q^2_u + Q^2_d)(\frac{11}{8} - \frac{3}{4}\log\frac{M^2_W}{\mu^2_{PW}})\right]$. In order to separate the FSR QED we can choose $\mu_{PW} = M_W \exp(-\frac{11}{12})$. This is in agreement with the corresponding treatment in PHOTOS.

III. OVERVIEW OF RECENT XFITTER RESULTS

A. W and Z Boson Production

In Reference [2], the xFitter collaboration (formerly HERAFitter) analyzed measurements of the W-boson charge asymmetry and of the Z-boson production cross sections, performed at the Tevatron collider in Run II by the D0 and CDF collaborations. Figure 1 shows the comparison of the relative uncertainty of the PDFs using the HERA I data alone, and together with the Tevatron W/Z data. This new data significantly reduces the PDF uncertainty, and this is most noticeable for the case of the d-valence, as shown.
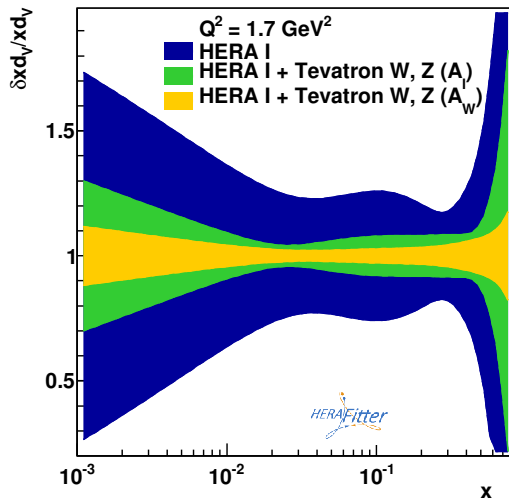
FIG. 1. We show the d-valence PDF relative uncertainty at $Q^2 = 1.7$ GeV^2 as a function of the Bjorken-x determined with a fit to the HERA I data (blue), HERA I and Tevatron W-boson asymmetry and Z-boson data (yellow), and HERA I and Tevatron W-boson lepton asymmetry and Z-boson data (green). Figure from Ref. [2].

FIG. 2. Comparison between the photon PDF $x\gamma(x, Q^2)$ at $Q^2 = 10^4$ GeV^2 from the present NNLO analysis (xFitter_epHMDY) with the corresponding results from NNPDF3.0qed [73], LUXqed [74] and HKR16 [75]. The PDF uncertainties are shown at the 68% CL obtained from the MC method, while model and parametrisation uncertainties are addressed separately. For HKR16 only the central value is shown, while for LUXqed the associated PDF uncertainty band is included. Figure from Ref. [25].

To study the possible model dependence due to the W-boson rapidity reconstruction, an alternative fit was performed in which the W-boson charge asymmetries measured by CDF and D0 were excluded, and the latest D0 measurement of the electron asymmetry was included. In Fig. 1, the fit to the lepton asymmetry data (green band) yields very compatible results to the W-boson asymmetry data (yellow band), but the uncertainties on the d_v PDF are up to twice as large.

These findings highlight the importance of the Tevatron W- and Z-boson production data to constrain the PDFs, and illustrate the utility of xFitter to easily demonstrate the impact of individual data sets. All the supporting material to allow fits of the Tevatron data, including the updated correlation model and the grid files for fast theory calculations, are publicly available on the xFitter web page.

B. The Photon PDF

Achieving the highest precision for theoretical predictions requires that the calculations include perturbative QCD corrections up to (N)NNLO, and electroweak (EW) corrections up to NLO. Working at this level of precision demands the QED effects are fully included, and this requires the introduction of the photon parton distribution of the proton, $x\gamma(x, Q^2)$.

To demonstrate these capabilities, Ref. [25] analyzed recent ATLAS measurements of high-mass Drell-Yan dilepton production at $\sqrt{s} = 8$ TeV to determine the photon PDF, and to compare it with some of the existing

determinations from the literature.

To include the photon PDF, xFitter links to the APFEL program [7] to incorporate NLO QED effects. The inclusion of NLO QED evolution effects are cross checked using the independent QEDEVOL [77] code based on the QCDNUM [6] evolution program. Additionally, the aMCfast interface [78] is used to include the photon-initiated contributions in the EW calculations within MadGraph5_aMC@NLO [79].

The resulting photon PDF determination represents an important validation of our understanding on the nature and implications of the photon PDF. Fig. 2 shows the results as compared with other recent QED fits. For $x \leq 0.1$, the four determinations of the photon PDF are consistent within uncertainties. For smaller values of x, the photon PDF from LUXqed and HKR16 is somewhat smaller than xFitter_epHMDY, but still in agreement at the 2-σ level. This agreement is further improved if the PDF uncertainties in xFitter_epHMDY arising from variations of the input parametrisation are added to experimental uncertainties. Moreover, the results of this work and NNPDF3.0QED agree at the 68% CL for $x \leq 0.03$, and the agreement extends to smaller values of x once the parametrisation uncertainties in xFitter_epHMDY are accounted for. The LUXqed and the HKR16 calculations of $x\gamma(x, Q^2)$ are very close to each other across the entire range of x.

The results of this study have been made possible by a number of technical developments that should be of
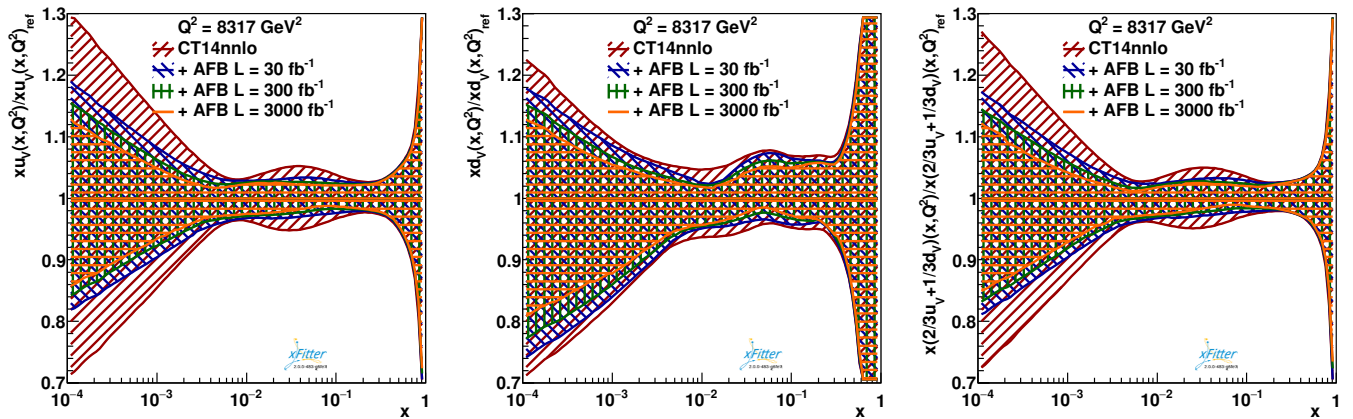
FIG. 3. A sample profiling comparison illustrating the impact of the A_{FB} data on the valence quark PDFs and their weighted sum for the original (red) and profiled (blue, green, orange) CT14nnlo [76] set. Figure from Ref. [3].

direct application for future PDF fits accounting for QED corrections. These technical improvements will certainly be helpful for future studies of the photon PDF of the proton.

C. The Forward-Backward Asymmetry in Neutral Current Drell-Yan Production

The DY-induced lepton charge asymmetry in charged current (CC) processes has been an effective way to constrain PDFs. Ref. [3] examines the use of neutral current (NC) lepton charge asymmetry measurements, which are traditionally used in the context of precision determinations of the weak mixing angle θ_W, to obtain improved PDF constraints.

Specifically, a forward-backward asymmetry A_{FB}^* is computed at NLO using the MadGraph5_aMC@NLO program [79] interfaced to APPLgrid [10] through aMCfast [78]. The A_{FB}^* is sensitive to valence quark PDFs through the combination of chiral couplings $(2/3 u_V + 1/3 d_V)$. The valence quark PDFs in turn also influence the sea PDF constraints via the sum rule relations.

For this study, three sets of pseudodata relevant for LHC Run 2, 3, and HL-LHC were considered. Fig 3 displays the impact of the data on the valence quark PDFs and their combination weighted by their electric charges, for 30, 300 and 3000 fb^{-1}. Comparing those profiled error bands, we note a visible improvement in the distribution of the valence quark PDFs, especially in the region of small x. Some improvement in the high x region of quark PDFs can be obtained employing sufficiently large data samples and applying suitable rapidity cuts on the A_{FB}^* observable.

This analysis illustrates how high-statistics measurements, both cross section and asymmetry distributions, from the LHC Runs 2, 3 and the HL-LHC stage can be exploited to place constraints on the
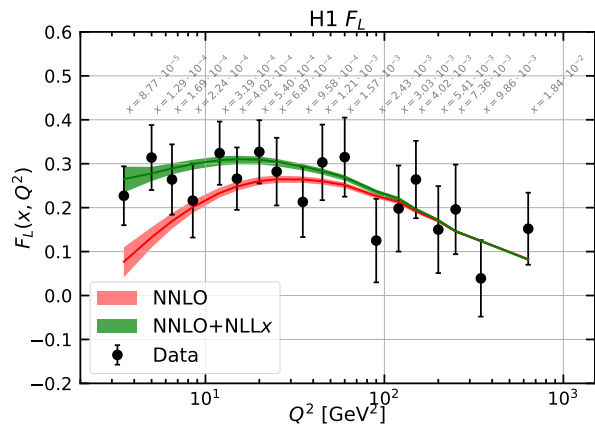
FIG. 4. The H1 extraction of F_L compared to the predictions with and without the $\ln(1/x)$ resummation (NLLx) contributions. Figure from Ref. [45].

PDFs. The PDF profiling calculations in the xFitter framework can flexibly be used to investigate the impact of pseudodata on PDF determinations.

D. Impact of low-x resummation on QCD analysis of HERA data

In Ref. [45], xFitter explored the impact of resumming the Next-to-Leading-Log $\ln(1/x)$ (NLLx) contributions in the small x region using a QCD analysis of HERA data. This work was prompted, in part, by the observation that the χ^2 of the NNLO fits was not improved as compared with the NLO fit for low values of Q^2.

This analysis used the final combined $e^{\pm}p$ cross-section measurements of H1 and ZEUS [80] which covered the kinematic range of Q^2 from 0.045 GeV^2 to 50000 GeV^2

and of Bjorken x from 0.65 down to 6×10^{-7}. Fits to this final combined HERA DIS cross-section data within the conventional DGLAP framework of QCD have shown some tension at low x and low Q^2. Our goal was to determine whether incorporating the $\ln(1/x)$-resummation terms into the HERAPDF fits might help resolve these tensions.

While the details are presented in Ref. [45], in brief it was observed that the total χ^2 for the fits improved from 1468/1207 for the NNLO fit, to 1394/1207 for the NNLO+NNLLx fit. The nominal improvement of the total χ^2 reflects the fact that the small x data is only a portion of the full data set; however, the impact in the small x region is significant as indicated in Fig. 4 where we see the $\ln(1/x)$ contributions yield an improved fit for the longitudinal structure function in the small x and low Q^2 region. The precise kinematic region where this resummation is important is delineated in Fig. 11 of Ref. [45].

Additionally, the resummation yields a larger gluon PDF in the small x and low Q^2 region, and this avoids potential problems due to a negative gluon PDF in forward physics. These features make PDFs with $\ln(1/x)$ resummation much more suitable for use in MC generators, such as Sherpa [81].

In conclusion, $\ln(1/x)$ resummation provides substantial improvement in the description of the precise HERA1+2 combined data. The NLLx contributions yield an improved description of the data, especially the longitudinal structure function F_L in the small x region, as compared to both the (un-resummed) NLO and NNLO analysis, and it also avoids potential problems of the negative gluon PDF at low x and Q^2.

E. Heavy quark matching scales: Unifying the FFNS and VFNS

High precision phenomenological analysis of DIS data requires a proper treatment of the heavy quarks mass scales. The Variable Flavor Number Scheme (VFNS) incorporates the heavy quark mass scale across the full kinematic range by varying the number of active flavors (N_F) in the DGLAP QCD evolution. In the VFNS, the matching scale μ_m determines the transition from N_F to $N_F + 1$ active flavors. Historically, μ_m was taken to be the heavy quark mass m_H; however, this choice is not required, and there are advantages to using a flexible matching scale. This feature is implemented in xFitter via the APFEL code, and we demonstrate the benefits in Ref. [82].

An essential element of this analysis is to implement the correction matching of the PDFs across the flavor threshold. The matching conditions have been computed to NLO and NNLO within the xFitter code, and the impact of this choice on the physical structure function $F_2^b(x, Q)$ is illustrated in Fig. 5. We emphasize some key features illustrated in the matching conditions.
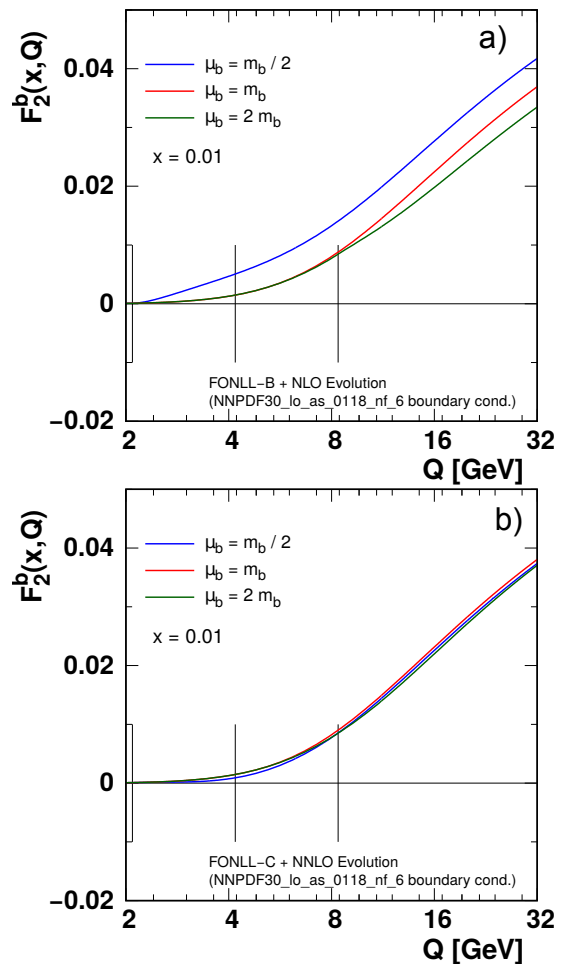
FIG. 5. The b-quark structure function $F_2^b(x, \mu)$ for different choices of the matching scales $\mu_m = \{m_b/2, m_b, 2m_b\}$ (indicated by the vertical lines) computed at NLO (Fig.-a) and NNLO (Fig.-b). Figure from Ref. [82].

At NLO (Fig. 5-a), we observe that there are sizeable differences for the three choices of matching scales, $\mu_b = \{m_b/2, m_b, 2m_b\}$. As the NLO matching conditions incorporate the $\mathcal{O}(\alpha_S)$ DGLAP evolution contributions, the differences of these curves simply reflects the NNLO $\mathcal{O}(\alpha_S^2)$ correction. Thus, when we compute the NNLO result (Fig. 5-b), we find the differences due to the matching scale are now significantly reduced as they are N³LO $\mathcal{O}(\alpha_S^3)$.

Ref. [82] illustrates the use of the variable matching scale for the case of heavy quark (charm and bottom) production at HERA. The flexibility of choosing the μ_m matching scale provides a number of advantages. By adjusting the matching scale, we can effectively transition between a VFNS and a FFNS in a seamless manner. For example, $\mu_m = m_b$ would correspond to the traditional VFNS, and $\mu_m \to \infty$ would correspond to the traditional FFNS. Furthermore we can choose any scale in between. Thus, the variable heavy flavor matching scale μ_m generalizes the transition between the FFNS

and the VFNS.

On a more practical level, this flexibility allows one to shift the matching scale so that the discontinuities associated with the N_F to $N_F + 1$ transition do not lie in the middle of a specific data set.

In summary, the flexibility of choosing the heavy flavor matching scale μ_m generalizes the transition between a FFNS and a VFNS, and provides a theoretical "laboratory" which can quantitatively test proposed implementations. The ability to vary the heavy flavor matching scales not only provides new insights into the intricacies of QCD, but also has practical advantages for PDF fits

F. Constraining the Strange PDF
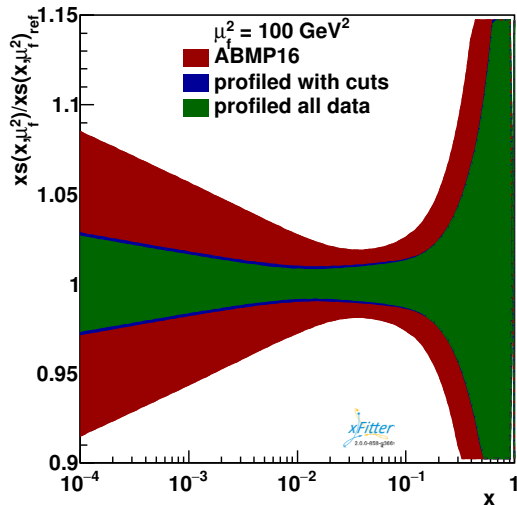
FIG. 6. The relative strange PDF uncertainty at $\mu_f^2 = 100$ GeV^2 of the original and profiled ABMP16 PDF set. Figure from Ref. [83].

The study of heavy quark production plays a critical role enabling us to fully characterize the properties of the SM. The charm quark is especially useful in this respect as the combination of fixed-target and collider data allow us to investigate the full kinematic spectrum from the threshold region ($m_c \sim Q$) to the asymptotic high energy limit ($m_c \ll Q$). Additionally, the charged-current charm production provides direct access to the strange quark distribution. The strange PDF is of particular interest because it still has large uncertainties despite being extensively investigated in a number of experiments such as inclusive W/Z production and $W + c$ associated production. Looking to the future, it is clearly important to reduce the uncertainty of the PDFs in general, and the strange-quark in particular, as we strive to make increasingly precise tests of the SM.

In Ref. [83], we used the xFitter framework to study charm production in charged-current deep-inelastic

scattering (DIS) using LHeC pseudodata to estimate the potential improvement from a future DIS facility. As xFitter implements both fixed-flavor- and variable-flavor-number schemes, we also compared the impact of these different theoretical choices to highlight several interesting aspects of multi-scale calculations.

For the LHeC parameters, we assumed a 7 TeV proton beam on a 60 GeV electron beam yielding $\sqrt{s} \sim 1.3$ TeV with a nominal design luminosity of 10^{33} cm^{-2} s^{-1}. Compared to HERA, this extends the covered kinematic range by an order of magnitude in both x_{Bj} and Q^2. The predictions are provided for unpolarized beams in the kinematic range $10^2 < Q^2 < 10^5$ GeV^2, $10^{-4} < x_{Bj} < 0.25$, and $0.0024 < y < 0.76$.

Using the high-statistics pseudodata with the xFitter analysis, we find strong constraints on the strange-quark PDF, especially in the previously unexplored small-x_{Bj} region. Figure 6 illustrates the relative improvement of the strange PDF uncertainty using the ABMP16 PDFs [84]. The general reduction of the PDF uncertainties is evident across the full x range. We also performed calculations using the NNPDF3.1 PDFs [85] and obtained similar conclusions.

As xFitter can compute in both the Fixed Flavor Number Scheme (FFNS) Variable Flavor Number Scheme (VFNS), we investigated the differences due the the scheme choice. We computed the reduced cross section using both the FFNS and VFNS, and then cut out those pseudodata where the scheme uncertainty was larger than the PDF uncertainty. In Fig. 6 this result (in blue) is labeled as "profiled with cuts." If we include all the data (labeled, "profiled all data") we obtain the uncertainty band labeled in green. Comparing these two results, we find that the pseudodata can impose very strong constraints on the PDFs and this is independent of the particular heavy-flavor scheme.

G. The Pion PDF

To further demonstrate the versatility of xFitter, Ref. [18] presented the first open-source analysis of parton distribution functions (PDFs) of charged pions. The pion is the simplest $q\bar{q}$ state in the quark-parton model of hadrons. However, despite this apparent simplicity, the pion structure is currently poorly understood, especially compared to the proton.

Experimentally, the pion PDF is known mostly from QCD analyses of Drell-Yan (DY) and prompt photon production data. This analysis used a combination of Drell-Yan (E615 and NA10) and prompt photon (WA70) data to provide constraints on both the quarks and gluons across the kinematic range.

The calculations are implemented at next-to-leading order (NLO) using APPLgrids generated by MCFM generator which allows for efficient numerical computations; additionally, modifications were made to APPLgrid which facilitate both meson and hadron
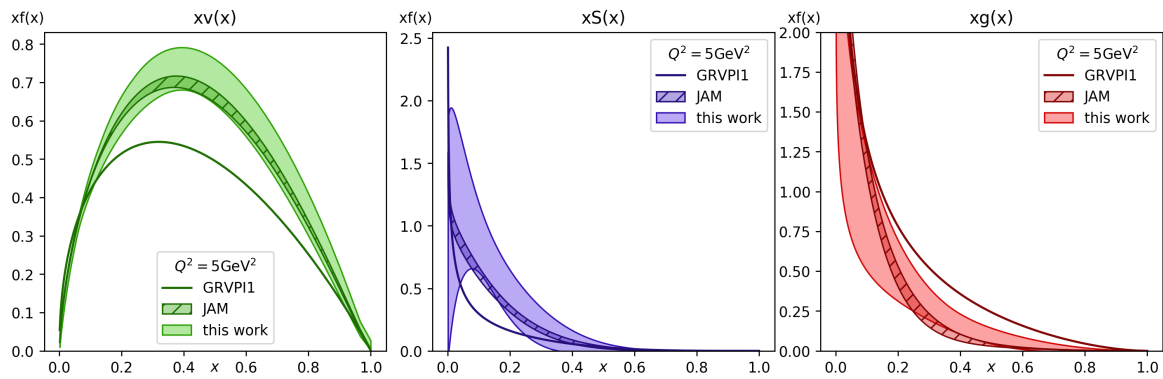
FIG. 7. Comparison between the pion PDFs obtained in this work, a determination by the JAM collaboration [86], and the GRVPI1 pion PDF set [87]. Figure from Ref. [18].

PDFs in the initial state.

Fig. 7 presents the fitted pion PDFs and compares with results from JAM [86] and GRVPI1 [87]. In general, the results obtained from xFitter compare favorably to JAM within uncertainties, but do show differences with the older GRV analysis. For the uncertainty bands, the μ_R and μ_F renormalization scales were varied, as well as the PDF parameter values. For the valence distribution, the dominant uncertainty is the scale variation, and this is rather well constrained. For the sea and gluon distributions, the calculation only included the direct photons in the model; hence, the missing fragmentation contribution to the prompt photon production process is the dominant uncertainty source. This is certainly an issue to be improved in a future analysis.

To further illustrate the flexibility of the xFitter framework, both a 3-parameter and 4-parameter form for the initial valence distribution was used. This type of parameter flexibility is crucial as it allows, for example, the investigation of the PDF slope in the large x limit.

While this study demonstrated the versatility of xFitter to perform meson PDF analysis, there are numerous directions this work can be extended. For example, new J/Ψ data could play an important role in constraining the gluon [88], and data from future experiments such as COMPASS++/AMBER [89], may allow for more flexible parameterizations and improved constraints.

H. The Pion Fragmentation Function

In addition to pion PDFs, xFitter can also compute pion fragmentation functions. Reference [90] presents the first open-source analysis of fragmentation functions of charged pions (entitled IPM-xFitter) computed at next-to-leading order (NLO) and next-to-next-to-leading order (NNLO) accuracy in perturbative QCD using the xFitter framework. This study incorporated a comprehensive set of pion production data from single-inclusive annihilation (SIA) processes, as well as the most
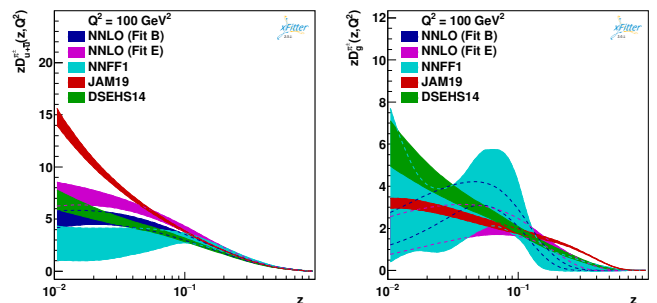
FIG. 8. Comparison of the preferred Fit E [IPMx] as well as Fit B for charged pion FFs ($\pi^+ + \pi^-$) at NNLO with NNFF1 [4] at NNLO, JAM19 [13] at NLO, DSEHS [5] at NLO for $Q^2 = 100\,\mathrm{GeV}^2$. Note, discretion is necessary when interpreting the very low z region; see text. Figure from Ref. [90].

recent measurements of inclusive cross-sections of single pion by the BELLE collaboration.

A primary goal of this analysis was to investigate the influence of the BELLE13 [91], BELLE20 [92], and BaBar [93] data sets on the resulting fragmentation functions. A total of five fits were generated using different data combinations and different kinematic cuts. 1) Fit A focused on the impact of the BELLE13 data set without BELLE20; 2) Fit B used the BELLE20 data set without BELLE13; 3) Fit C used the BELLE20 data set without BaBar; 4) Fit D focused the impact of the BELLE20 data set without either BELLE13 or BaBar, and imposed a $z > 0.2$ cut on the BELLE20; 5) Fit E excluded BELLE13 but included BELLE20 with a $z > 0.2$ cut, and BaBar with a $z > 0.1$ cut.

Comparisons of selected fits are displayed in Fig. 8 along with results from the literature. The different fits are in reasonable agreement for larger z values, but begin to diverge for smaller z. Note, discretion is necessary when interpreting the very low z region as the extrapolation of the fragmentation function grids extends beyond the region fitted in the individual analyses. For example, the JAM19 focus was on SIDIS in the region

$z \gtrsim 0.2$, and NNFF1 used a lower kinematic cut of z_{min}=0.02 for $Q = M_Z$ and 0.075 for $Q < M_Z$. While Fit E is our preferred fit, we also display Fit B to highlight the impact of the low z cuts.

This study generally found good quality for the fits across most of the z range, but the description of the data in the low-z region remains an unresolved puzzle. The resulting NLO and NNLO pion FFs provide valuable insights for applications in present and future high-energy analysis of pion final state processes.

Contemporaneous with the above study, a related investigation was reported in Ref. [94] using a complementary neural-network approach with different data sets; this opens new avenues for future study and may help resolve some of the issues in the small z region.

IV.   APPLICATIONS OF xFitter

A.   Usage of xFitter by LHC Collaborations

xFitter is the standard tool for QCD analyses by the ATLAS and CMS Collaborations at the LHC, resulting in a number of different studies.

xFitter has been used to quantify the sensitivity to PDFs of differential W and Z bosons [95–98] and of W+charm quark [99, 100] cross-section measurements, showing how they provide important constraints on the strangeness content of the proton. Other studies have illustrated the gluon PDF sensitivity of $t\bar{t}$ cross-sections measurements [101–103]. An ATLAS study [104] highlighted cross-section ratios, such as for $t\bar{t}/Z$ measured at different energies, as a powerful quantity to probe the gluon/sea PDF ratio free of large experimental uncertainties.

The xFitter capabilities to perform coherent analysis of PDFs plus additional parameters of interest, has been exploited to measure SM parameters which correlate with PDFs. The $t\bar{t}$ cross-sections have been used for extractions of the top quark mass [105–107], which for the CMS analyses has been done simultaneously with a determination of the strong coupling and of the PDFs. Simultaneous extractions of the strong coupling with the PDFs have been performed by CMS also from inclusive jets [108, 109] and dijet [110] cross-sections, recently extended to determinations of the contribution of SMEFT operators introducing new four-fermion interactions simultaneously with the PDFs [109].

In Ref. [97], high precision measurements of the inclusive differential $W^{\pm}$ and Z/γ^* boson cross sections at 7 TeV were added to the HERA data, resulting in the PDF set **ATLASepWZ16**, which improved on the HERAPDF2.0 set in various respects. Firstly, the strange content of the sea was determined rather than assumed to be a fixed fraction of the light sea. Indeed, compared to previous determinations, the strange sea was found to be enhanced at low x. Secondly, the accuracy of the valence quark distributions for $x < 0.1$

was improved.

In Ref. [111], the ATLAS Collaboration performed a PDF fit including for the first time measurements for the production of W and Z boson in association with a jet, resulting in the **ATLASepWZVjets20** PDF set. The V + jets data are sensitive to partons at higher x than can be accessed by inclusive $W, Z/\gamma^*$ data and, in particular, they constrain the $\bar{d}$ and $\bar{s}$ quarks at higher x.

And more recently an ATLAS PDF fit [112] was performed including a variety of measurements of different production processes (Drell-Yan, V+jets, direct photon production, $t\bar{t}$ and inclusive jets data) at different center-of-mass energies. The resulting set of PDFs is called **ATLASpdf21**.

B.   Nuclear PDFs with xFitter
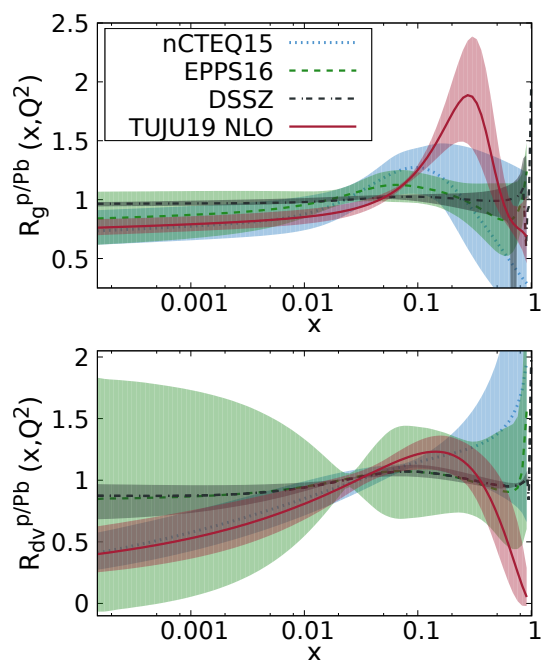
FIG. 9. Selected nuclear PDF ratios for lead as compared to proton at NLO for TUJU19 [17], nCTEQ15 [113], EPPS16 [114], and DSSZ [115] at $Q^2 = 100$ GeV^2. Figures from Ref. [17].

Reference [17] extended xFitter to include the capability of performing fits to nuclear PDFs, and generated a new set of nPDFs (TUJU19) at both NLO and NNLO. While this extension is capable of performing a simultaneous fit to both the proton and nuclear degrees of freedom, to ensure stability they first generated a proton baseline derived with a very similar setup as for the HERA2.0 PDFs [80], and then used this as the starting point for the nPDF investigation. Both charged-lepton and neutrino DIS data sets wer included, and and isoscalar corrections and correlated uncertainties were also incorporated.

The necessary modifications to the xFitter code were

extensive. The PDF parameterization was extended to include the nuclear A dimension; this increased the number of fitting parameters, and these changes were propagated throughout the code (e.g., in the steering file and the MINUIT interface). The nuclear data sets depend on the nuclear A and Z, so this information was provided within the data files and the input/output routines were modified accordingly. Finally, the DGLAP evolution code was modified to evolve nuclear PDFs covering different combinations of A and Z individually. These modifications included a new numerical integration routine to accommodate the flexibility of an A-dependent normalization.

This work highlights the versatility and flexibility of the xFitter program, and this study serves as a foundation for a wide variety other investigations involving nuclear interactions. The details of this work are presented in Ref. [17], and the code is available on GitLab.[2]

C. Higgs Physics with xFitter

Precision studies in the Higgs sector of the Standard Model (SM) are central to current [116] and forthcoming [117] physics programs at the LHC. The dominant mechanism for the production of Higgs bosons in pp collisions at the LHC is given by gluon fusion. With the very high accuracy reached in perturbative QCD calculations of Higgs production cross sections, currently of next-to-next-to-next-to-leading order (N^{3}LO) [118] in the QCD coupling α_s, the theoretical systematic uncertainties on the predictions for Higgs boson production are strongly influenced by the gluon PDF, as well as the sea-quark PDFs coupled to gluons through initial-state QCD evolution. The PDF contribution is estimated [117] to be about 30% of the total uncertainty, including α_s and scale variations.

The primary source of knowledge of the gluon PDF is provided at present by HERA deep inelastic scattering (DIS) experimental measurements. While future DIS experiments [14–16] are proposed to extend the range and accuracy of our current knowledge of the gluon PDF, substantial progress can also come from measurements at the LHC itself, particularly in the forthcoming high-luminosity phase HL-LHC [119]. Gluon PDF studies have been considered so far from the analysis of light-quark jets [120], open [65, 121] and bound-state [122] charm and bottom quark production, top quark production [123]. These studies rely on parton-level processes with colored particles in the lowest-order final state, which are influenced by large radiative corrections. Ref. [4] proposes an alternative approach,

based on considering color-singlet production at the LHC, and (analogously to the case of DIS at HERA) achieving sensitivity to the gluon PDF through $\mathcal{O}(\alpha_s)$ contributions, guided by criteria of perturbative stability and experimental precision.

Drell-Yan (DY) lepton pair production via electroweak vector boson exchange is one of the most precisely measured processes at the LHC. The DY cross section summed over the vector-boson polarizations is sensitive to the gluon PDF for finite vector-boson transverse momenta p_T. However, in the p_T region where the cross section is largest, it is affected by large perturbative corrections to all orders in α_s (see e.g. [26], and references therein). Ref. [4] therefore turns to the contributions of the individual polarizations of the vector boson. It exploits the sensitivity of the DY angular coefficient A_0 associated with the longitudinal vector-boson polarization to the gluon PDF in order to constrain the Higgs boson cross section from gluon fusion. The coefficient A_0 is perturbatively stable, as illustrated by the smallness of its next-to-leading-order (NLO) and next-to-next-to-leading-order (NNLO) [124] radiative corrections for finite p_T, and precisely measured at the LHC [125, 126]. With xFitter, we can investigate in detail the impact of precision measurements of the longitudinally-polarized vector-boson coefficient A_0 on the theoretical predictions for the Higgs boson production cross section. These studies can further be extended, using xFitter, to other DY angular coefficients, since additional sensitivity may be gained from longitudinal-transverse polarization interferences, as in the parity-conserving A_1 and parity-violating A_3 coefficients.

An example illustrating the implications of the longitudinally polarized A_0 coefficient on the Higgs boson production is shown in Fig. 10 [4] versus the Higgs boson rapidity y_H. The SM Higgs boson production is computed in the gluon fusion mode for $\sqrt{s} = 13$ TeV pp collisions, using the MCFM code [127] at NLO in QCD perturbation theory. We evaluate PDF uncertainties on the Higgs cross section including constraints obtained with xFitter from A_0 profiling near the Z-boson mass. We see that in the region $-2 \lesssim y_H \lesssim 2$ the uncertainty is reduced by about 30 - 40 % in the Run III scenario, and a further reduction to about 50 % takes place in the HL-LHC scenario.

In Fig. 11 [4] we perform a higher-order N^{3}LO calculation for the Higgs boson total cross section using the code ggHiggs [129, 130]. We report the result for the cross section and its uncertainty in the cases of the current CT18nnlo [128], NNPDF3.1nnlo [85] and MSHT20nnlo [131] global sets as well as projected sets, based on complete LHC data sample [132]. The PDF4LHC15scen1/2 sets, which are PDF projections including HL-LHC pseudodata, also show a smaller, but not negligible, reduction in uncertainties. Notwithstanding the numerical differences, the behavior is qualitatively similar for the different sets, and provides
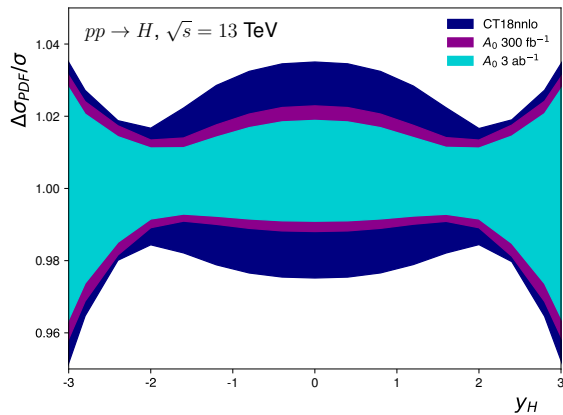

FIG. 10. Ratio of PDF uncertainties for the gluon-gluon fusion SM Higgs boson cross-section in pp collisions at $\sqrt{s} =$ 13 TeV as a function of the Higgs rapidity [4]. The blue band shows the uncertainties of the CT18nnlo PDF set [128], reduced to 68% CL coverage. The red and green bands show the uncertainties of the CT18nnlo including constraints from the A_0 measurement and assuming 300 fb^{-1} and 3 ab^{-1}, respectively.
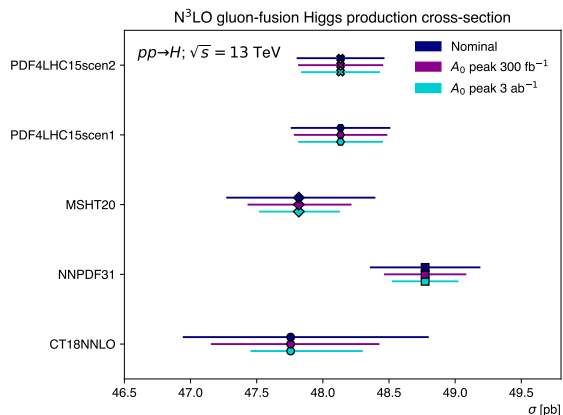

FIG. 11. The gluon-gluon fusion Higgs boson production cross-section [4] at N^{3}LO for different PDFs, showing the uncertainty from PDFs and their expected reduction including constraints from the A_0 measurement assuming 300 fb^{-1} and 3 ab^{-1}, respectively.

further support at N^{3}LO to the picture given in Fig. 10 for the NLO Higgs boson rapidity cross section.

The approach illustrated above can be extended to mass regions away from the Z peak, where it has the potential to provide complementary physics information. High-mass DY angular distributions allow the region of larger x momentum fractions to be accessed and will be relevant for associated Higgs boson production with a gauge/Higgs boson or heavy-flavour quarks. Measurements of A_0 at low masses may be used to probe p_T dependent gluon PDF effects, influencing the

Higgs boson p_T spectrum for low transverse momenta and ratios of Higgs to DY p_T spectra [133], as well as the small-x regime [130, 134] of Higgs boson production relevant to the highest energy frontier [135].

D. BSM Physics with xFitter

The capabilities of xFitter can be exploited for studies of new physics beyond the Standard Model (BSM).

Consider for instance BSM experimental searches at the LHC in dielectron/dimuon channels and charged lepton plus missing transverse energy channels. These are classic methods to search for new Z'/W' gauge bosons: see for example the analyses by ATLAS in Refs. [136, 137] and by CMS in Refs. [138, 139]. Such searches will be further pursued at the High-Luminosity LHC (HL-LHC) [140].

In the case of BSM scenarios with narrow vector resonances one can rely on traditional "bump search" analyses based on the Breit-Wigner (BW) lineshape. In the case of BSM scenarios featuring vector resonances with large width, on the other hand, the default bump searches are likely not sufficient: instead of an easily observable narrow BW lineshape, the resonance appears as a broad shoulder spreading over the SM background. Alternative experimental approaches can be applied to the case of wide resonances, in which one has to exploit the tails of the measured mass distributions. Examples of such approaches include for instance "counting strategy" analyses. These approaches are much more dependent than bump searches on the modeling of the dominant production process [141], for both signal and background.

Then, in the case of wide-resonance searches the role of PDFs becomes prominent as one of the main sources of theoretical systematic uncertainties, because it directly affects our ability to test BSM scenarios and the experimental sensitivity to new physics. This thus influences the potential of experimental searches for discovering or setting exclusion bounds on heavy BSM states.

In the multi-TeV region of W'/Z' masses defined by the current LHC exclusion limits [136–139], quark distributions in the valence sector dominate the PDF systematics. With an xFitter profiling analysis, Ref. [142] finds that the valence quark systematics can be improved by combining high-precision measurements of Charged Current (CC) and Neutral Current (NC) Drell-Yan asymmetries in the mass region near the SM weak boson poles. This exploits the sensitivity of the NC forward-backward asymmetry A_{FB} to the charge-weighted linear combination $(2/3)u_V + (1/3)d_V$ of up-quark and down-quark valence distributions [3] and the sensitivity of the CC lepton-charge asymmetry A_W to the difference $u_V - d_V$. The constraints from the A_{FB} and A_W combination at the SM weak boson mass scale, examined in the two projected luminosity scenarios of 300 fb^{-1} (for the LHC Run 3) and of 3000 fb^{-1} (for the HL-LHC [140]), turn

out to improve the relative PDF uncertainties by up to around 20% [142] in the region of the invariant and transverse mass spectra between 2 TeV and 6 TeV, in which evidence for W' and/or Z' states with large widths could first be observed.

We can then analyze quantitatively how the "improved PDFs", obtained from the reduction of the valence PDF uncertainty due to $A_{\rm FB}$ and A_W precision measurements at the SM weak boson mass scale, result into an enhancement of the experimental sensitivity to BSM searches at the TeV scale. In the next subsection we illustrate this with a specific example.

In this kind of analysis, an important feature, stemming from multi-resonant profiles of mass spectra and influencing the experimental search strategies, is the following. Strong interference effects between the BSM resonances themselves and between the BSM and SM states can give rise to a statistically significant depletion of events below the BW peak in the invariant mass distribution, leading to the appearance of a pronounced *dip* [141, 142]. It is possible to define the significance of the depletion of events in a manner similar to that for the excess of events of the peak, which can be used to extract model dependent exclusion and discovery limits in the model's parameter space. One can then present such limits resulting from the analysis of the spectra for either the peak or the dip. The xFitter framework enables one to investigate whether the peak or the dip analyses especially benefit from the "improved PDFs".

We next turn to the specific example of BSM W'/Z' states in composite Higgs models, considering broad-resonance searches in the leptonic channels. For sensitivity studies comparing leptonic with heavy-quark channels in composite Higgs models see e.g. [143].

1. Enhancing the sensitivity of BSM searches with improved PDFs

New gauge sectors in strongly-coupled models of electroweak symmetry breaking [144] based on composite Nambu-Goldstone Higgs [145, 146] feature multiple W' and Z' broad resonances, and interference effects of the heavy bosons with each other and with SM gauge bosons. An example is the 4-Dimensional Composite Higgs Model (4DCHM) realization [147] of the minimal composite Higgs model of Ref. [148]. The parameter space of the model can be characterized in terms of two parameters, the compositeness scale f and the coupling g_ρ of the new resonances, with the resonances mass scale being of order $M \sim f g_\rho$ [144, 149]. Ref. [150] selects two 4DCHM benchmarks, denoted by A and B, each characterized by specific values of f, g_ρ and the resonance masses. We next present an example of the results for exclusion and discovery limits in the parameter space of these two 4DCHM benchmarks which can be obtained by using the "improved PDFs" [142].

In Fig. 12 [150] we show the limits from NC Drell-Yan on the model parameter space, described in terms of f and g_ρ, for the HL-LHC stage with center-of-mass energy of 14 TeV and an integrated luminosity of 3000 fb^{-1}. In the background we give contour plots for the masses of the new gauge bosons. The blue and red curves are obtained respectively with the baseline CT18NNLO PDF set [128] and with the profiled PDFs [142] using the $A_{\rm FB}$ and A_W combination with 3000 fb^{-1} of integrated luminosity. The top panel in Fig. 12 is for the peak analysis, the bottom panel is for the dip analysis. In this setup, the peak of benchmark A would still be below the experimental sensitivity, while the peak of benchmark B, if the improved PDFs are employed, would be right below the 2σ exclusion. When exploiting the depletion of events in the dip below the peak, the sensitivity on the model increases remarkably. Furthermore, as visible from the bottom plot of Fig. 12, the improvement on the PDF also has a very large impact particularly in the region of small f and large g_ρ, where the sensitivity on the dip can overtake the LHC reach in the peak region once the profiled PDFs are employed. Taking into account the reduction of PDF uncertainty, benchmark A would be now at the edge of the 5σ discovery, while the sensitivity on benchmark B would almost reach 3σ.

Tab. I [150] lists, in the case of the two benchmarks A and B, the integration intervals in invariant mass for the dip region as well as the resulting cross sections for the SM background and the complete 4DCHM, together with the associated PDF uncertainty using the baseline CT18NNLO PDF set [128] and the profiled version [142] using the $A_{\rm FB}$ and A_W combination with 3000 fb^{-1} of integrated luminosity. It reports also the obtained significances for an integrated luminosity of 3000 fb^{-1} employing the two PDF errors. The improvement in significance due to the profiled PDFs is sizeable, as significances grow by an amount from 40% to 90% (i.e., by a factor of about 10 in comparison) for the benchmarks A and B, respectively. A more modest improvement in significance is found [150] in the case of the peak.

The above studies can be extended to CC Drell-Yan. In fact, it is noted in [150] that, for cases in which both neutral and charged new states appear and are correlated by theory, the reduction of systematic PDF error can profitably be applied to combined W' and Z' searches. For example, in the 4DCHM a direct W' exclusion (or indeed discovery) achieved in the CC channel can be used indirectly to probe the existence of a Z' better than this can be done with direct searches in the NC channel. The analysis of the dip often provides more stringent limits than the signal coming from the peak, with the reduction of systematic PDF errors playing a crucial part in this conclusion.
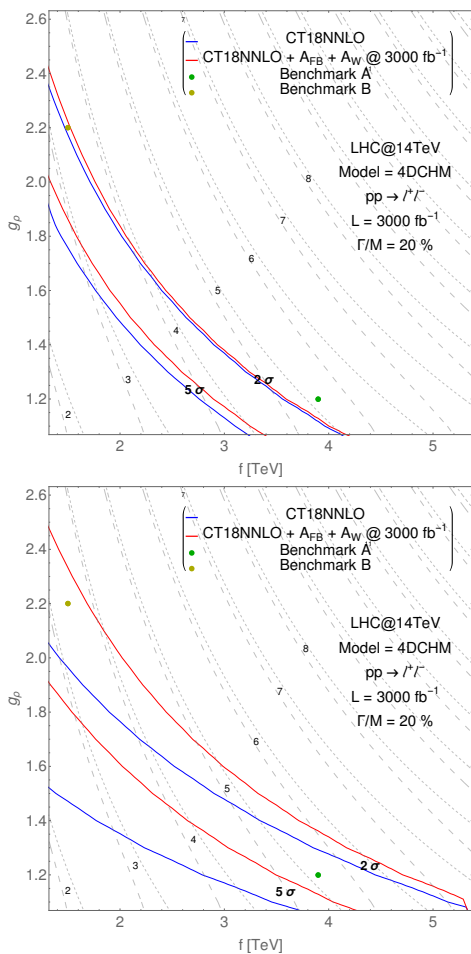
FIG. 12. Exclusion and discovery limits at 3000 fb^{-1} for the peak (top) and for the dip (bottom) for Z' resonances with $\Gamma/M = 20\%$ [150]. The short (long) dashed contours give the BSM boson mass M_{Z_2} ($M_{Z_3} \simeq M_{W_2}$) in TeV.

2. Applications with SMEFT

In the discussion of the previous subsection, we study the impact of "improved" PDFs on BSM physics at the multi-TeV scale, while the improvement itself in the PDFs comes from processes at the SM weak boson mass scale. The asymmetry pseudodata employed in the profiling [142] are centered around the SM vector boson peaks and take into account only SM contributions. Since we consider TeV scale BSM resonances, the new physics contribution to the forward-backward asymmetry A_{FB} at the weak scale, which is due to the interference between SM and BSM process, is small, and a similar conclusion holds for the charged-current differential cross section distribution.

On the other hand, a different scenario arises

if one includes data or pseudodata in the PDF determination which do contain contamination from BSM contributions. This is the case, for example,

Benchmark A			
inf [TeV]	sup [TeV]	σ_{SM} [fb]	$\sigma_{\mathrm{SM+BSM}}$ [fb]
2.06	4.99	$1.69 \cdot 10^{-1}$	$1.42 \cdot 10^{-1}$
Δ_{PDF} base [fb]	Δ_{PDF} profiled [fb]	α (base)	α (profiled)
$9.5 \cdot 10^{-3}$	$4.6 \cdot 10^{-3}$	3.34	4.82

Benchmark B			
inf [TeV]	sup [TeV]	σ_{SM} [fb]	$\sigma_{\mathrm{SM+BSM}}$ [fb]
1.36	3.36	1.53	1.45
Δ_{PDF} base [fb]	Δ_{PDF} profiled [fb]	α (base)	α (profiled)
$6.8 \cdot 10^{-2}$	$3.1 \cdot 10^{-2}$	1.53	2.91

TABLE I. Integration limits for the dip region, integrated cross section for the SM background and the complete model and its PDF uncertainty with the baseline CT18NNLO PDF set and the profiled PDF set using $A_{\mathrm{FB}} + A_W$ pseudodata as well as the significances α employing the two PDF errors for an integrated luminosity of 3000 fb^{-1} for the benchmarks A and B [150].

of data or pseudodata at high mass scales in the multi-TeV region. In this case, assuming purely SM predictions would lead to biased estimations on new physics constraints: see for instance the recent studies [109, 151].

This bias can be avoided if the PDFs are extracted simultaneously with the BSM parameters. Such non-biased approaches are feasible with xFitter via interfaces to BSM computations, for instance by using SM effective field theory (SMEFT) expansions. For example, the CIJET [152, 153] interface allows extending jet cross sections with dimension-6 SMEFT operators for purely left-handed, vector-like or axial vector-like color-singlet exchanges. An xFitter analysis in this direction is underway.

V. CONCLUSION

The xFitter program is a versatile, flexible, modular, and comprehensive tool that can facilitate analyses of the experimental data and theoretical calculations.

It is a valuable framework for bench-marking and understanding differences between PDF fits, and it can provide impact studies for possible future facilities including HL-LHC, EIC, LHeC, DUNE, and UHE Cosmic Ray experiments. We encourage use of xFitter, and welcome new contributions from the community to ensure xFitter continues to incorporate the latest theoretical advances and precision experimental data.

[1] S. Alekhin *et al.*, "HERAFitter," *Eur. Phys. J. C* **75** no. 7, (2015) 304, `arXiv:1410.4412 [hep-ph]`.

[2] **HERAFitter developers' Team** Collaboration, S. Camarda *et al.*, "QCD analysis of *W*- and *Z*-boson production at Tevatron," *Eur. Phys. J. C* **75** no. 9, (2015) 458, `arXiv:1503.05221 [hep-ph]`.

[3] E. Accomando *et al.*, "PDF Profiling Using the Forward-Backward Asymmetry in Neutral Current Drell-Yan Production," *JHEP* **10** (2019) 176, `arXiv:1907.07727 [hep-ph]`.

[4] S. Amoroso, J. Fiaschi, F. Giuli, A. Glazov, F. Hautmann, and O. Zenaiev, "Longitudinal Z-boson polarization and the Higgs boson production cross section at the Large Hadron Collider," *Phys. Lett. B* **821** (2021) 136613, `arXiv:2012.10298 [hep-ph]`.

[5] **xFitter Developers' Team** Collaboration, V. Bertone *et al.*, "xFitter 2.0.0: An Open Source QCD Fit Framework," *PoS* **DIS2017** (2018) 203, `arXiv:1709.01151 [hep-ph]`.

[6] M. Botje, "QCDNUM: Fast QCD Evolution and Convolution," *Comput. Phys. Commun.* **182** (2011) 490–532, `arXiv:1005.1481 [hep-ph]`.

[7] V. Bertone, S. Carrazza, and J. Rojo, "APFEL: A PDF Evolution Library with QED corrections," *Comput. Phys. Commun.* **185** (2014) 1647–1668, `arXiv:1310.1394 [hep-ph]`.

[8] V. Bertone, "APFEL++: A new PDF evolution library in C++," *PoS* **DIS2017** (2018) 201, `arXiv:1708.00911 [hep-ph]`.

[9] A. Buckley, J. Ferrando, S. Lloyd, K. Nordström, B. Page, M. Rüfenacht, M. Schönherr, and G. Watt, "LHAPDF6: parton density access in the LHC precision era," *Eur. Phys. J. C* **75** (2015) 132, `arXiv:1412.7420 [hep-ph]`.

[10] T. Carli, D. Clements, A. Cooper-Sarkar, C. Gwenlan, G. P. Salam, F. Siegert, P. Starovoitov, and M. Sutton, "A posteriori inclusion of parton density functions in NLO QCD final-state calculations at hadron colliders: The APPLGRID Project," *Eur. Phys. J. C* **66** (2010) 503–524, `arXiv:0911.2985 [hep-ph]`.

[11] V. Bertone, S. Carrazza, and N. P. Hartland, "APFELgrid: a high performance tool for parton density determinations," *Comput. Phys. Commun.* **212** (2017) 205–209, `arXiv:1605.02070 [hep-ph]`.

[12] D. Britzger, G. S. Klaus Rabbertz, F. Stober, and M. Wobisch, "Recent Developments of the fastNLO Toolkit," *PoS* **DIS2015** (2015) 055.

[13] M. Aliev, H. Lacker, U. Langenfeld, S. Moch, P. Uwer, and M. Wiedermann, "HATHOR: HAdronic Top and Heavy quarks crOss section calculatoR," *Comput. Phys. Commun.* **182** (2011) 1034–1046, `arXiv:1007.1327 [hep-ph]`.

[14] **LHeC, FCC-he Study Group** Collaboration, P. Agostini *et al.*, "The Large Hadron-Electron Collider at the HL-LHC," *J. Phys. G* **48** no. 11, (2021) 110501, `arXiv:2007.14491 [hep-ex]`.

[15] A. Accardi *et al.*, "Electron Ion Collider: The Next QCD Frontier: Understanding the glue that binds us all," *Eur. Phys. J. A* **52** no. 9, (2016) 268, `arXiv:1212.1701 [nucl-ex]`.

[16] *Proceedings, Probing Nucleons and Nuclei in High Energy Collisions: Dedicated to the Physics of the Electron Ion Collider: Seattle (WA), United States, October 1 - November 16, 2018.* WSP, 2, 2020. `arXiv:2002.12333 [hep-ph]`.

[17] M. Walt, I. Helenius, and W. Vogelsang, "Open-source QCD analysis of nuclear parton distribution functions at NLO and NNLO," *Phys. Rev. D* **100** no. 9, (2019) 096015, `arXiv:1908.03355 [hep-ph]`.

[18] I. Novikov *et al.*, "Parton Distribution Functions of the Charged Pion Within The xFitter Framework," *Phys. Rev. D* **102** no. 1, (2020) 014040, `arXiv:2002.02902 [hep-ph]`.

[19] **xFitter Developers' Team** Collaboration, H. Abdolmaleki *et al.*, "Probing the strange content of the proton with charm production in charged current at LHeC," *Eur. Phys. J. C* **79** no. 10, (2019) 864, `arXiv:1907.01014 [hep-ph]`.

[20] H. Abdolmaleki *et al.*, "Forward-Backward Drell-Yan Asymmetry and PDF Determination," in *54th Rencontres de Moriond on QCD and High Energy Interactions*, pp. 211–214. ARISF, 7, 2019. `arXiv:1907.08301 [hep-ph]`.

[21] E. Accomando, J. Fiaschi, F. Hautmann, and S. Moretti, "Neutral current forward–backward asymmetry: from θ_W to PDF determinations," *Eur. Phys. J. C* **78** no. 8, (2018) 663, `arXiv:1805.09239 [hep-ph]`. [Erratum: Eur.Phys.J.C 79, 453 (2019)].

[22] E. Accomando, J. Fiaschi, F. Hautmann, and S. Moretti, "Constraining Parton Distribution Functions from Neutral Current Drell-Yan Measurements," *Phys. Rev. D* **98** no. 1, (2018) 013003, `arXiv:1712.06318 [hep-ph]`. [Erratum: Phys.Rev.D 99, 079902 (2019)].

[23] E. Accomando, J. Fiaschi, F. Hautmann, S. Moretti, and C. H. Shepherd-Themistocleous, "Photon-initiated production of a dilepton final state at the LHC: Cross section versus forward-backward asymmetry studies," *Phys. Rev. D* **95** no. 3, (2017) 035014, `arXiv:1606.06646 [hep-ph]`.

[24] E. Accomando, J. Fiaschi, F. Hautmann, S. Moretti, and C. H. Shepherd-Themistocleous, "The effect of real and virtual photons in the di-lepton channel at the LHC," *Phys. Lett. B* **770** (2017) 1–7, `arXiv:1612.08168 [hep-ph]`.

[25] **xFitter Developers' Team** Collaboration, F. Giuli *et al.*, "The photon PDF from high-mass Drell–Yan data at the LHC," *Eur. Phys. J. C* **77** no. 6, (2017) 400, `arXiv:1701.08553 [hep-ph]`.

[26] R. Angeles-Martinez *et al.*, "Transverse Momentum Dependent (TMD) parton distribution functions: status and prospects," *Acta Phys. Polon. B* **46** no. 12, (2015) 2501–2534, `arXiv:1507.05267 [hep-ph]`.

[27] F. Hautmann and H. Jung, "Transverse momentum dependent gluon density from DIS precision data," *Nucl. Phys. B* **883** (2014) 1–19, `arXiv:1312.7875 [hep-ph]`.

[28] S. Dooling, F. Hautmann, and H. Jung, "Hadroproduction of electroweak gauge boson plus jets and TMD parton density functions," *Phys. Lett. B* **736** (2014) 293–298, `arXiv:1406.2994 [hep-ph]`.

[29] F. Hautmann, H. Jung, and S. T. Monfared, "The

CCFM uPDF evolution uPDFevolv Version 1.0.00," *Eur. Phys. J. C* **74** (2014) 3082, `arXiv:1407.5935 [hep-ph]`.

[30] A. Bermudez Martinez, P. Connor, H. Jung, A. Lelek, R. Žlebčík, F. Hautmann, and V. Radescu, "Collinear and TMD parton densities from fits to precision DIS measurements in the parton branching method," *Phys. Rev. D* **99** no. 7, (2019) 074008, `arXiv:1804.11152 [hep-ph]`.

[31] F. Hautmann, H. Jung, A. Lelek, V. Radescu, and R. Zlebcik, "Collinear and TMD Quark and Gluon Densities from Parton Branching Solution of QCD Evolution Equations," *JHEP* **01** (2018) 070, `arXiv:1708.03279 [hep-ph]`.

[32] F. Hautmann, H. Jung, A. Lelek, V. Radescu, and R. Zlebcik, "Soft-gluon resolution scale in QCD evolution equations," *Phys. Lett. B* **772** (2017) 446–451, `arXiv:1704.01757 [hep-ph]`.

[33] F. Hautmann, H. Jung, M. Krämer, P. J. Mulders, E. R. Nocera, T. C. Rogers, and A. Signori, "TMDlib and TMDplotter: library and plotting tools for transverse-momentum-dependent parton distributions," *Eur. Phys. J. C* **74** (2014) 3220, `arXiv:1408.3015 [hep-ph]`.

[34] N. A. Abdulov *et al.*, "TMDlib2 and TMDplotter: a platform for 3D hadron structure studies," *Eur. Phys. J. C* **81** no. 8, (2021) 752, `arXiv:2103.09741 [hep-ph]`.

[35] S. Catani and F. Hautmann, "High-energy factorization and small x deep inelastic scattering beyond leading order," *Nucl. Phys. B* **427** (1994) 475–524, `arXiv:hep-ph/9405388`.

[36] E. A. Kuraev, L. N. Lipatov, and V. S. Fadin, "Multi - Reggeon Processes in the Yang-Mills Theory," *Sov. Phys. JETP* **44** (1976) 443–450.

[37] E. A. Kuraev, L. N. Lipatov, and V. S. Fadin, "The Pomeranchuk Singularity in Nonabelian Gauge Theories," *Sov. Phys. JETP* **45** (1977) 199–204.

[38] I. I. Balitsky and L. N. Lipatov, "The Pomeranchuk Singularity in Quantum Chromodynamics," *Sov. J. Nucl. Phys.* **28** (1978) 822–829.

[39] T. Jaroszewicz, "Gluonic Regge Singularities and Anomalous Dimensions in QCD," *Phys. Lett. B* **116** (1982) 291–294.

[40] S. Catani and F. Hautmann, "Quark anomalous dimensions at small x," *Phys. Lett. B* **315** (1993) 157–163.

[41] V. S. Fadin and L. N. Lipatov, "BFKL pomeron in the next-to-leading approximation," *Phys. Lett. B* **429** (1998) 127–134, `arXiv:hep-ph/9802290`.

[42] M. Ciafaloni and G. Camici, "Energy scale(s) and next-to-leading BFKL equation," *Phys. Lett. B* **430** (1998) 349–354, `arXiv:hep-ph/9803389`.

[43] M. Bonvini, S. Marzani, and T. Peraro, "Small-x resummation from HELL," *Eur. Phys. J. C* **76** no. 11, (2016) 597, `arXiv:1607.02153 [hep-ph]`.

[44] M. Bonvini, S. Marzani, and C. Muselli, "Towards parton distribution functions with small-x resummation: HELL 2.0," *JHEP* **12** (2017) 117, `arXiv:1708.07510 [hep-ph]`.

[45] **xFitter Developers' Team** Collaboration, H. Abdolmaleki *et al.*, "Impact of low-x resummation on QCD analysis of HERA data," *Eur. Phys. J. C* **78** no. 8, (2018) 621, `arXiv:1802.00064 [hep-ph]`.

[46] M. Bonvini and F. Giuli, "A new simple PDF parametrization: improved description of the HERA data," *Eur. Phys. J. Plus* **134** no. 10, (2019) 531, `arXiv:1902.11125 [hep-ph]`.

[47] **xFitter Developers' Team** Collaboration, V. Bertone *et al.*, "A determination of $m_c(m_c)$ from HERA data using a matched heavy-flavor scheme," *JHEP* **08** (2016) 050, `arXiv:1605.01946 [hep-ph]`.

[48] K. J. Golec-Biernat and M. Wusthoff, "Saturation effects in deep inelastic scattering at low Q**2 and its implications on diffraction," *Phys. Rev. D* **59** (1998) 014017, `arXiv:hep-ph/9807513`.

[49] J. Bartels, K. J. Golec-Biernat, and H. Kowalski, "A modification of the saturation model: DGLAP evolution," *Phys. Rev. D* **66** (2002) 014001, `arXiv:hep-ph/0203258`.

[50] E. Iancu, K. Itakura, and S. Munier, "Saturation and BFKL dynamics in the HERA data at small x," *Phys. Lett. B* **590** (2004) 199–208, `arXiv:hep-ph/0310338`.

[51] A. Luszczak and H. Kowalski, "Dipole model analysis of high precision HERA data," *Phys. Rev. D* **89** no. 7, (2014) 074051, `arXiv:1312.4060 [hep-ph]`.

[52] A. Luszczak and H. Kowalski, "Dipole model analysis of highest precision HERA data, including very low Q^2's," *Phys. Rev. D* **95** no. 1, (2017) 014030, `arXiv:1611.10100 [hep-ph]`.

[53] A. Łuszczak and W. Schäfer, "Incoherent diffractive photoproduction of J/ψ and Υ on heavy nuclei in the color dipole approach," *Phys. Rev. C* **97** no. 2, (2018) 024903, `arXiv:1712.04502 [hep-ph]`.

[54] A. Łuszczak and W. Schäfer, "Coherent photoproduction of J/ψ in nucleus-nucleus collisions in the color dipole approach," *Phys. Rev. C* **99** no. 4, (2019) 044905, `arXiv:1901.07989 [hep-ph]`.

[55] A. M. Cooper-Sarkar and K. Wichmann, "QCD analysis of the ATLAS and CMS $W^{\pm}$ and Z cross-section measurements and implications for the strange sea density," *Phys. Rev. D* **98** no. 1, (2018) 014027, `arXiv:1803.00968 [hep-ex]`.

[56] **ATLAS** Collaboration, M. Aaboud *et al.*, "Precision measurement and interpretation of inclusive W^+ , W^- and Z/γ^* production cross sections with the ATLAS detector," *Eur. Phys. J. C* **77** no. 6, (2017) 367, `arXiv:1612.03016 [hep-ex]`.

[57] **ATLAS** Collaboration, G. Aad *et al.*, "Measurement of the production of a W boson in association with a charm quark in pp collisions at $\sqrt{s} = 7$ TeV with the ATLAS detector," *JHEP* **05** (2014) 068, `arXiv:1402.6263 [hep-ex]`.

[58] **CMS** Collaboration, S. Chatrchyan *et al.*, "Measurement of Associated W + Charm Production in pp Collisions at $\sqrt{s} = 7$ TeV," *JHEP* **02** (2014) 013, `arXiv:1310.1138 [hep-ex]`.

[59] R. Abdul Khalek *et al.*, "Science Requirements and Detector Concepts for the Electron-Ion Collider: EIC Yellow Report," `arXiv:2103.05419 [physics.ins-det]`.

[60] C. A. Argüelles *et al.*, "New opportunities at the next-generation neutrino experiments I: BSM neutrino physics and dark matter," *Rept. Prog. Phys.* **83** no. 12, (2020) 124201, `arXiv:1907.08311 [hep-ph]`.

[61] **NuSTEC** Collaboration, L. Alvarez-Ruso *et al.*, "NuSTEC White Paper: Status and challenges of neutrino–nucleus scattering," *Prog. Part. Nucl. Phys.*

100 (2018) 1–68, `arXiv:1706.03621 [hep-ph]`.

[62] **IceCube** Collaboration, M. G. Aartsen *et al.*, "Observation and Characterization of a Cosmic Muon Neutrino Flux from the Northern Hemisphere using six years of IceCube data," *Astrophys. J.* **833** no. 1, (2016) 3, `arXiv:1607.08006 [astro-ph.HE]`.

[63] **IceCube** Collaboration, M. G. Aartsen *et al.*, "Evidence for High-Energy Extraterrestrial Neutrinos at the IceCube Detector," *Science* **342** (2013) 1242856, `arXiv:1311.5238 [astro-ph.HE]`.

[64] A. Bhattacharya, R. Enberg, Y. S. Jeong, C. S. Kim, M. H. Reno, I. Sarcevic, and A. Stasto, "Prompt atmospheric neutrino fluxes: perturbative QCD models and nuclear effects," *JHEP* **11** (2016) 167, `arXiv:1607.00193 [hep-ph]`.

[65] **PROSA** Collaboration, O. Zenaiev, M. V. Garzelli, K. Lipka, S. O. Moch, A. Cooper-Sarkar, F. Olness, A. Geiser, and G. Sigl, "Improved constraints on parton distributions using LHCb, ALICE and HERA heavy-flavour measurements and implications for the predictions for prompt atmospheric-neutrino fluxes," *JHEP* **04** (2020) 118, `arXiv:1911.13164 [hep-ph]`.

[66] S. Agarwal, K. Mierle, and Others, "Ceres solver." `http://ceres-solver.org`.

[67] **H1** Collaboration, V. Andreev *et al.*, "Determination of electroweak parameters in polarised deep-inelastic scattering at HERA," *Eur. Phys. J. C* **78** no. 9, (2018) 777, `arXiv:1806.01176 [hep-ex]`.

[68] D. Britzger, M. Klein, and H. Spiesberger, "Electroweak physics in inclusive deep inelastic scattering at the LHeC," *Eur. Phys. J. C* **80** no. 9, (2020) 831, `arXiv:2007.11799 [hep-ph]`.

[69] F. Hautmann, L. Keersmaekers, A. Lelek, and A. M. Van Kampen, "Dynamical resolution scale in transverse momentum distributions at the LHC," *Nucl. Phys. B* **949** (2019) 114795, `arXiv:1908.08524 [hep-ph]`.

[70] S. Camarda *et al.*, "DYTurbo: Fast predictions for Drell-Yan processes," *Eur. Phys. J. C* **80** no. 3, (2020) 251, `arXiv:1910.07049 [hep-ph]`. [Erratum: Eur.Phys.J.C 80, 440 (2020)].

[71] V. Bertone, G. Bozzi, and F. Hautmann, "Perturbative hysteresis and emergent resummation scales," *Phys. Rev. D* **105** no. 9, (2022) 096003, `arXiv:2202.03380 [hep-ph]`.

[72] V. Bertone, G. Bozzi, and F. Hautmann, "Resummation Scales and the Assessment of Theoretical Uncertainties in Parton Distribution Functions," in *29th International Workshop on Deep-Inelastic Scattering and Related Subjects.* 5, 2022. `arXiv:2205.15900 [hep-ph]`.

[73] **NNPDF** Collaboration, R. D. Ball *et al.*, "Parton distributions for the LHC Run II," *JHEP* **04** (2015) 040, `arXiv:1410.8849 [hep-ph]`.

[74] A. Manohar, P. Nason, G. P. Salam, and G. Zanderighi, "How bright is the proton? A precise determination of the photon parton distribution function," *Phys. Rev. Lett.* **117** no. 24, (2016) 242002, `arXiv:1607.04266 [hep-ph]`.

[75] L. A. Harland-Lang, V. A. Khoze, and M. G. Ryskin, "The photon PDF in events with rapidity gaps," *Eur. Phys. J. C* **76** no. 5, (2016) 255, `arXiv:1601.03772 [hep-ph]`.

[76] S. Dulat, T.-J. Hou, J. Gao, M. Guzzi, J. Huston, P. Nadolsky, J. Pumplin, C. Schmidt, D. Stump, and C. P. Yuan, "New parton distribution functions from a global analysis of quantum chromodynamics," *Phys. Rev. D* **93** no. 3, (2016) 033006, `arXiv:1506.07443 [hep-ph]`.

[77] R. Sadykov, "Impact of QED radiative corrections on Parton Distribution Functions," `arXiv:1401.1133 [hep-ph]`.

[78] V. Bertone, R. Frederix, S. Frixione, J. Rojo, and M. Sutton, "aMCfast: automation of fast NLO computations for PDF fits," *JHEP* **08** (2014) 166, `arXiv:1406.7693 [hep-ph]`.

[79] J. Alwall, R. Frederix, S. Frixione, V. Hirschi, F. Maltoni, O. Mattelaer, H. S. Shao, T. Stelzer, P. Torrielli, and M. Zaro, "The automated computation of tree-level and next-to-leading order differential cross sections, and their matching to parton shower simulations," *JHEP* **07** (2014) 079, `arXiv:1405.0301 [hep-ph]`.

[80] **H1, ZEUS** Collaboration, H. Abramowicz *et al.*, "Combination of measurements of inclusive deep inelastic $e^{\pm}p$ scattering cross sections and QCD analysis of HERA data," *Eur. Phys. J. C* **75** no. 12, (2015) 580, `arXiv:1506.06042 [hep-ex]`.

[81] T. Gleisberg, S. Hoeche, F. Krauss, M. Schonherr, S. Schumann, F. Siegert, and J. Winter, "Event generation with SHERPA 1.1," *JHEP* **02** (2009) 007, `arXiv:0811.4622 [hep-ph]`.

[82] **xFitter Developers Team** Collaboration, V. Bertone *et al.*, "Impact of the heavy quark matching scales in PDF fits," *Eur. Phys. J. C* **77** no. 12, (2017) 837, `arXiv:1707.05343 [hep-ph]`.

[83] **xFitter Developers' Team** Collaboration, H. Abdolmaleki *et al.*, "Probing the strange content of the proton with charm production in charged current at LHeC," *Eur. Phys. J. C* **79** no. 10, (2019) 864, `arXiv:1907.01014 [hep-ph]`.

[84] S. Alekhin, J. Blümlein, and S. Moch, "NLO PDFs from the ABMP16 fit," *Eur. Phys. J. C* **78** no. 6, (2018) 477, `arXiv:1803.07537 [hep-ph]`.

[85] **NNPDF** Collaboration, R. D. Ball *et al.*, "Parton distributions from high-precision collider data," *Eur. Phys. J. C* **77** no. 10, (2017) 663, `arXiv:1706.00428 [hep-ph]`.

[86] P. C. Barry, N. Sato, W. Melnitchouk, and C.-R. Ji, "First Monte Carlo Global QCD Analysis of Pion Parton Distributions," *Phys. Rev. Lett.* **121** no. 15, (2018) 152001, `arXiv:1804.01965 [hep-ph]`.

[87] M. Gluck, E. Reya, and A. Vogt, "Pionic parton distributions," *Z. Phys. C* **53** (1992) 651–656.

[88] W.-C. Chang, J.-C. Peng, S. Platchkov, and T. Sawada, "Constraining gluon density of pions at large x by pion-induced J/ψ production," *Phys. Rev. D* **102** no. 5, (2020) 054024, `arXiv:2006.06947 [hep-ph]`.

[89] B. Adams *et al.*, "Letter of Intent: A New QCD facility at the M2 beam line of the CERN SPS (COMPASS++/AMBER)," `arXiv:1808.00848 [hep-ex]`.

[90] **xfitter Developers' Team** Collaboration, H. Abdolmaleki, M. Soleymaninia, H. Khanpour, S. Amoroso, F. Giuli, A. Glazov, A. Luszczak, F. Olness, and O. Zenaiev, "QCD analysis of pion fragmentation functions in the xFitter framework,"

Phys. Rev. D **104** no. 5, (2021) 056019,
`arXiv:2105.11306 [hep-ph]`.

[91] **Belle** Collaboration, M. Leitgab *et al.*, "Precision
Measurement of Charged Pion and Kaon Differential
Cross Sections in e+e- Annihilation at s=10.52 GeV,"
Phys. Rev. Lett. **111** (2013) 062002, `arXiv:1301.6183`
`[hep-ex]`.

[92] **Belle** Collaboration, R. Seidl *et al.*, "Update of
inclusive cross sections of single and pairs of identified
light charged hadrons," *Phys. Rev. D* **101** no. 9,
(2020) 092004, `arXiv:2001.10194 [hep-ex]`.

[93] **BaBar** Collaboration, J. P. Lees *et al.*, "Production of
charged pions, kaons, and protons in e^+e^-
annihilations into hadrons at $\sqrt{s}$=10.54 GeV," *Phys.
Rev. D* **88** (2013) 032011, `arXiv:1306.2895 [hep-ex]`.

[94] R. A. Khalek, V. Bertone, and E. R. Nocera,
"Determination of unpolarized pion fragmentation
functions using semi-inclusive deep-inelastic-scattering
data," *Phys. Rev. D* **104** no. 3, (2021) 034007,
`arXiv:2105.08725 [hep-ph]`.

[95] **ATLAS** Collaboration, G. Aad *et al.*, "Determination
of the strange quark density of the proton from
ATLAS measurements of the $W \to \ell\nu$ and $Z \to \ell\ell$
cross sections," *Phys. Rev. Lett.* **109** (2012) 012001,
`arXiv:1203.4051 [hep-ex]`.

[96] **CMS** Collaboration, S. Chatrchyan *et al.*,
"Measurement of the Muon Charge Asymmetry in
Inclusive $pp \to W + X$ Production at $\sqrt{s} = 7$ TeV and
an Improved Determination of Light Parton
Distribution Functions," *Phys. Rev. D* **90** no. 3, (2014)
032004, `arXiv:1312.6283 [hep-ex]`.

[97] **ATLAS** Collaboration, M. Aaboud *et al.*, "Precision
measurement and interpretation of inclusive W^+ , W^-
and Z/γ^* production cross sections with the ATLAS
detector," *Eur. Phys. J. C* **77** no. 6, (2017) 367,
`arXiv:1612.03016 [hep-ex]`.

[98] **CMS** Collaboration, V. Khachatryan *et al.*,
"Measurement of the differential cross section and
charge asymmetry for inclusive pp $\to$ W$^{\pm}$ + X
production at $\sqrt{s} = 8$ TeV," *Eur. Phys. J. C* **76** no. 8,
(2016) 469, `arXiv:1603.01803 [hep-ex]`.

[99] **CMS** Collaboration, A. M. Sirunyan *et al.*,
"Measurement of associated production of a W boson
and a charm quark in proton-proton collisions at $\sqrt{s} =$
13 TeV," *Eur. Phys. J. C* **79** no. 3, (2019) 269,
`arXiv:1811.10021 [hep-ex]`.

[100] **CMS** Collaboration, A. Tumasyan *et al.*,
"Measurements of the associated production of a W
boson and a charm quark in proton-proton collisions at
$\sqrt{s} = 8$ TeV," `arXiv:2112.00895 [hep-ex]`.

[101] **CMS** Collaboration, A. M. Sirunyan *et al.*,
"Measurement of double-differential cross sections for
top quark pair production in pp collisions at $\sqrt{s} = 8$
TeV and impact on parton distribution functions,"
Eur. Phys. J. C **77** no. 7, (2017) 459,
`arXiv:1703.01630 [hep-ex]`.

[102] **CMS** Collaboration, A. M. Sirunyan *et al.*,
"Measurement of the inclusive t$\bar{\text{t}}$ cross section in pp
collisions at $\sqrt{s} = 5.02$ TeV using final states with at
least one charged lepton," *JHEP* **03** (2018) 115,
`arXiv:1711.03143 [hep-ex]`.

[103] **ATLAS** Collaboration, "Determination of the parton
distribution functions of the proton from ATLAS
measurements of differential W and Z/γ^* and $t\bar{t}$ cross

sections,".

[104] **ATLAS** Collaboration, M. Aaboud *et al.*,
"Measurements of top-quark pair to Z-boson
cross-section ratios at $\sqrt{s} = 13, 8, 7$ TeV with the
ATLAS detector," *JHEP* **02** (2017) 117,
`arXiv:1612.03636 [hep-ex]`.

[105] **ATLAS** Collaboration, M. Aaboud *et al.*,
"Measurement of lepton differential distributions and
the top quark mass in $t\bar{t}$ production in pp collisions at
$\sqrt{s} = 8$ TeV with the ATLAS detector," *Eur. Phys. J.
C* **77** no. 11, (2017) 804, `arXiv:1709.09407 [hep-ex]`.

[106] **CMS** Collaboration, A. M. Sirunyan *et al.*,
"Measurement of the t$\bar{\text{t}}$ production cross section, the
top quark mass, and the strong coupling constant
using dilepton events in pp collisions at $\sqrt{s} = 13$ TeV,"
Eur. Phys. J. C **79** no. 5, (2019) 368,
`arXiv:1812.10505 [hep-ex]`.

[107] **CMS** Collaboration, A. M. Sirunyan *et al.*,
"Measurement of t$\bar{\text{t}}$ normalised multi-differential cross
sections in pp collisions at $\sqrt{s} = 13$ TeV, and
simultaneous determination of the strong coupling
strength, top quark pole mass, and parton distribution
functions," *Eur. Phys. J. C* **80** no. 7, (2020) 658,
`arXiv:1904.05237 [hep-ex]`.

[108] **CMS** Collaboration, V. Khachatryan *et al.*,
"Measurement and QCD analysis of double-differential
inclusive jet cross sections in pp collisions at $\sqrt{s} = 8$
TeV and cross section ratios to 2.76 and 7 TeV,"
JHEP **03** (2017) 156, `arXiv:1609.05331 [hep-ex]`.

[109] **CMS** Collaboration, A. Tumasyan *et al.*,
"Measurement and QCD analysis of double-differential
inclusive jet cross sections in proton-proton collisions
at $\sqrt{s} = 13$ TeV," *JHEP* **02** (2022) 142,
`arXiv:2111.10431 [hep-ex]`.

[110] **CMS** Collaboration, A. M. Sirunyan *et al.*,
"Measurement of the triple-differential dijet cross
section in proton-proton collisions at $\sqrt{s} = 8$ TeV and
constraints on parton distribution functions," *Eur.
Phys. J. C* **77** no. 11, (2017) 746, `arXiv:1705.02628`
`[hep-ex]`.

[111] **ATLAS** Collaboration, G. Aad *et al.*, "Determination
of the parton distribution functions of the proton from
ATLAS measurements of differential W$^{\pm}$ and Z boson
production in association with jets," *JHEP* **07** (2021)
223, `arXiv:2101.05095 [hep-ex]`.

[112] **ATLAS** Collaboration, G. Aad *et al.*, "Determination
of the parton distribution functions of the proton using
diverse ATLAS data from pp collisions at $\sqrt{s} = 7, 8$
and 13 TeV," *Eur. Phys. J. C* **82** no. 5, (2022) 438,
`arXiv:2112.11266 [hep-ex]`.

[113] K. Kovarik *et al.*, "nCTEQ15 - Global analysis of
nuclear parton distributions with uncertainties in the
CTEQ framework," *Phys. Rev. D* **93** no. 8, (2016)
085037, `arXiv:1509.00792 [hep-ph]`.

[114] K. J. Eskola, P. Paakkinen, H. Paukkunen, and C. A.
Salgado, "EPPS16: Nuclear parton distributions with
LHC data," *Eur. Phys. J. C* **77** no. 3, (2017) 163,
`arXiv:1612.05741 [hep-ph]`.

[115] D. de Florian, R. Sassot, P. Zurita, and M. Stratmann,
"Global Analysis of Nuclear Parton Distributions,"
Phys. Rev. D **85** (2012) 074028, `arXiv:1112.6324`
`[hep-ph]`.

[116] **LHC Higgs Cross Section Working Group**
Collaboration, D. de Florian *et al.*, "Handbook of LHC

Higgs Cross Sections: 4. Deciphering the Nature of the Higgs Sector," arXiv:1610.07922 [hep-ph].

[117] M. Cepeda *et al.*, "Report from Working Group 2: Higgs Physics at the HL-LHC and HE-LHC," *CERN Yellow Rep. Monogr.* **7** (2019) 221–584, arXiv:1902.00134 [hep-ph].

[118] X. Chen, T. Gehrmann, E. W. N. Glover, A. Huss, B. Mistlberger, and A. Pelloni, "Fully Differential Higgs Boson Production to Third Order in QCD," *Phys. Rev. Lett.* **127** no. 7, (2021) 072002, arXiv:2102.07607 [hep-ph].

[119] P. Azzi *et al.*, "Report from Working Group 1: Standard Model Physics at the HL-LHC and HE-LHC," *CERN Yellow Rep. Monogr.* **7** (2019) 1–220, arXiv:1902.04070 [hep-ph].

[120] R. Abdul Khalek *et al.*, "Phenomenology of NNLO jet production at the LHC and its impact on parton distributions," *Eur. Phys. J. C* **80** no. 8, (2020) 797, arXiv:2005.11327 [hep-ph].

[121] M. Cacciari, M. L. Mangano, and P. Nason, "Gluon PDF constraints from the ratio of forward heavy-quark production at the LHC at $\sqrt{S} = 7$ and 13 TeV," *Eur. Phys. J. C* **75** no. 12, (2015) 610, arXiv:1507.06197 [hep-ph].

[122] C. A. Flett, S. P. Jones, A. D. Martin, M. G. Ryskin, and T. Teubner, "How to include exclusive J/ψ production data in global PDF analyses," *Phys. Rev. D* **101** no. 9, (2020) 094011, arXiv:1908.08398 [hep-ph].

[123] M. Czakon, N. P. Hartland, A. Mitov, E. R. Nocera, and J. Rojo, "Pinning down the large-x gluon with NNLO top-quark pair differential distributions," *JHEP* **04** (2017) 044, arXiv:1611.08609 [hep-ph].

[124] R. Gauld, A. Gehrmann-De Ridder, T. Gehrmann, E. W. N. Glover, and A. Huss, "Precise predictions for the angular coefficients in Z-boson production at the LHC," *JHEP* **11** (2017) 003, arXiv:1708.00008 [hep-ph].

[125] **CMS** Collaboration, V. Khachatryan *et al.*, "Angular coefficients of Z bosons produced in pp collisions at $\sqrt{s}$ = 8 TeV and decaying to $\mu^+\mu^-$ as a function of transverse momentum and rapidity," *Phys. Lett. B* **750** (2015) 154–175, arXiv:1504.03512 [hep-ex].

[126] **ATLAS** Collaboration, G. Aad *et al.*, "Measurement of the angular coefficients in Z-boson events using electron and muon pairs from data taken at $\sqrt{s} = 8$ TeV with the ATLAS detector," *JHEP* **08** (2016) 159, arXiv:1606.00689 [hep-ex].

[127] J. Campbell and T. Neumann, "Precision Phenomenology with MCFM," *JHEP* **12** (2019) 034, arXiv:1909.09117 [hep-ph].

[128] T.-J. Hou *et al.*, "New CTEQ global analysis of quantum chromodynamics with high-precision data from the LHC," *Phys. Rev. D* **103** no. 1, (2021) 014013, arXiv:1912.10053 [hep-ph].

[129] M. Bonvini, R. D. Ball, S. Forte, S. Marzani, and G. Ridolfi, "Updated Higgs cross section at approximate N^3LO," *J. Phys. G* **41** (2014) 095002, arXiv:1404.3204 [hep-ph].

[130] M. Bonvini and S. Marzani, "Double resummation for Higgs production," *Phys. Rev. Lett.* **120** no. 20, (2018) 202003, arXiv:1802.07758 [hep-ph].

[131] S. Bailey, T. Cridge, L. A. Harland-Lang, A. D. Martin, and R. S. Thorne, "Parton distributions from

LHC, HERA, Tevatron and fixed target data: MSHT20 PDFs," *Eur. Phys. J. C* **81** no. 4, (2021) 341, arXiv:2012.04684 [hep-ph].

[132] R. Abdul Khalek, S. Bailey, J. Gao, L. Harland-Lang, and J. Rojo, "Towards Ultimate Parton Distributions at the High-Luminosity LHC," *Eur. Phys. J. C* **78** no. 11, (2018) 962, arXiv:1810.03639 [hep-ph].

[133] P. Cipriano, S. Dooling, A. Grebenyuk, P. Gunnellini, F. Hautmann, H. Jung, and P. Katsas, "Higgs boson as a gluon trigger," *Phys. Rev. D* **88** no. 9, (2013) 097501, arXiv:1308.1655 [hep-ph].

[134] F. Hautmann, "Heavy top limit and double logarithmic contributions to Higgs production at m(H)**2 / s much less than 1," *Phys. Lett. B* **535** (2002) 159–162, arXiv:hep-ph/0203140.

[135] R. Contino *et al.*, "Physics at a 100 TeV pp collider: Higgs and EW symmetry breaking studies," arXiv:1606.09408 [hep-ph].

[136] **ATLAS** Collaboration, G. Aad *et al.*, "Search for high-mass dilepton resonances using 139 fb^{-1} of pp collision data collected at $\sqrt{s} =$13 TeV with the ATLAS detector," *Phys. Lett. B* **796** (2019) 68–87, arXiv:1903.06248 [hep-ex].

[137] **ATLAS** Collaboration, G. Aad *et al.*, "Search for a heavy charged boson in events with a charged lepton and missing transverse momentum from pp collisions at $\sqrt{s} = 13$ TeV with the ATLAS detector," *Phys. Rev. D* **100** no. 5, (2019) 052013, arXiv:1906.05609 [hep-ex].

[138] **CMS** Collaboration, A. M. Sirunyan *et al.*, "Search for high-mass resonances in dilepton final states in proton-proton collisions at $\sqrt{s} = 13$ TeV," *JHEP* **06** (2018) 120, arXiv:1803.06292 [hep-ex].

[139] **CMS** Collaboration, A. M. Sirunyan *et al.*, "Search for resonant and nonresonant new phenomena in high-mass dilepton final states at $\sqrt{s} = 13$ TeV," *JHEP* **07** (2021) 208, arXiv:2103.02708 [hep-ex].

[140] X. Cid Vidal *et al.*, "Report from Working Group 3: Beyond the Standard Model physics at the HL-LHC and HE-LHC," *CERN Yellow Rep. Monogr.* **7** (2019) 585–865, arXiv:1812.07831 [hep-ph].

[141] E. Accomando, F. Coradeschi, T. Cridge, J. Fiaschi, F. Hautmann, S. Moretti, C. Shepherd-Themistocleous, and C. Voisey, "Production of Z'-boson resonances with large width at the LHC," *Phys. Lett. B* **803** (2020) 135293, arXiv:1910.13759 [hep-ph].

[142] J. Fiaschi, F. Giuli, F. Hautmann, and S. Moretti, "Lepton-Charge and Forward-Backward Asymmetries in Drell-Yan Processes for Precision Electroweak Measurements and New Physics Searches," *Nucl. Phys. B* **968** (2021) 115444, arXiv:2103.10224 [hep-ph].

[143] D. Liu, L.-T. Wang, and K.-P. Xie, "Broad composite resonances and their signals at the LHC," *Phys. Rev. D* **100** no. 7, (2019) 075021, arXiv:1901.01674 [hep-ph].

[144] G. Panico and A. Wulzer, *The Composite Nambu-Goldstone Higgs*, vol. 913. Springer, 2016. arXiv:1506.01961 [hep-ph].

[145] D. B. Kaplan and H. Georgi, "SU(2) x U(1) Breaking by Vacuum Misalignment," *Phys. Lett. B* **136** (1984) 183–186.

[146] D. B. Kaplan, H. Georgi, and S. Dimopoulos, "Composite Higgs Scalars," *Phys. Lett. B* **136** (1984)

187–190.

[147] S. De Curtis, M. Redi, and A. Tesi, "The 4D Composite Higgs," *JHEP* **04** (2012) 042, `arXiv:1110.1613 [hep-ph]`.

[148] K. Agashe, R. Contino, and A. Pomarol, "The Minimal composite Higgs model," *Nucl. Phys. B* **719** (2005) 165–187, `arXiv:hep-ph/0412089`.

[149] G. F. Giudice, C. Grojean, A. Pomarol, and R. Rattazzi, "The Strongly-Interacting Light Higgs," *JHEP* **06** (2007) 045, `arXiv:hep-ph/0703164`.

[150] J. Fiaschi, F. Giuli, F. Hautmann, and S. Moretti, "Enhancing the Large Hadron Collider sensitivity to charged and neutral broad resonances of new gauge sectors," *JHEP* **02** (2022) 179, `arXiv:2111.09698`

`[hep-ph]`.

[151] A. Greljo, S. Iranipour, Z. Kassabov, M. Madigan, J. Moore, J. Rojo, M. Ubiali, and C. Voisey, "Parton distributions in the SMEFT from high-energy Drell-Yan tails," *JHEP* **07** (2021) 122, `arXiv:2104.02723 [hep-ph]`.

[152] J. Gao, C. S. Li, and C. P. Yuan, "NLO QCD Corrections to dijet Production via Quark Contact Interactions," *JHEP* **07** (2012) 037, `arXiv:1204.4773 [hep-ph]`.

[153] J. Gao, "CIJET: A program for computation of jet cross sections induced by quark contact interactions at hadron colliders," *Comput. Phys. Commun.* **184** (2013) 2362–2366, `arXiv:1301.7263 [hep-ph]`.